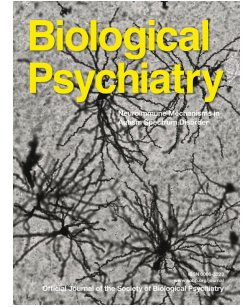


Journal Pre-proof



CDK5-dependent BAG3 degradation modulates synaptic protein turnover

Jiechao Zhou, Hei-Man Chow, Yan Liu, Di Wu, Meng Shi, Jieyin Li, Lei Wen, Yuehong Gao, Guimiao Chen, Kai Zhuang, Hui Lin, Guanyun Zhang, Wenting Xie, Huifang Li, Lige Leng, Mengdan Wang, Naizhen Zheng, Hao Sun, Yingjun Zhao, Yunwu Zhang, Maoqiang Xue, Timothy Y. Huang, Guojun Bu, Huaxi Xu, Zengqiang Yuan, Karl Herrup, Jie Zhang

PII: S0006-3223(19)31865-7

DOI: <https://doi.org/10.1016/j.biopsych.2019.11.013>

Reference: BPS 14057

To appear in: *Biological Psychiatry*

Received Date: 25 January 2019

Revised Date: 7 November 2019

Accepted Date: 8 November 2019

Please cite this article as: Zhou J., Chow H.-M., Liu Y., Wu D., Shi M., Li J., Wen L., Gao Y., Chen G., Zhuang K., Lin H., Zhang G., Xie W., Li H., Leng L., Wang M., Zheng N., Sun H., Zhao Y., Zhang Y., Xue M., Huang T.Y., Bu G., Xu H., Yuan Z., Herrup K. & Zhang J., CDK5-dependent BAG3 degradation modulates synaptic protein turnover, *Biological Psychiatry* (2019), doi: <https://doi.org/10.1016/j.biopsych.2019.11.013>.

This is a PDF file of an article that has undergone enhancements after acceptance, such as the addition of a cover page and metadata, and formatting for readability, but it is not yet the definitive version of record. This version will undergo additional copyediting, typesetting and review before it is published in its final form, but we are providing this version to give early visibility of the article. Please note that, during the production process, errors may be discovered which could affect the content, and all legal disclaimers that apply to the journal pertain.

© 2019 Published by Elsevier Inc on behalf of Society of Biological Psychiatry.

CDK5-dependent BAG3 degradation modulates synaptic protein turnover

Jiechao Zhou^{1,*}, Hei-Man Chow^{2,*,#}, Yan Liu^{1,4,*}, Di Wu^{1,*}, Meng Shi^{1,*}, Jieyin Li^{1,*}, Lei Wen^{1,4,*}, Yuehong Gao¹, Guimiao Chen¹, Kai Zhuang¹, Hui Lin¹, Guanyun Zhang¹, Wenting Xie¹, Huifang Li¹, Lige Leng¹, Mengdan Wang¹, Naizhen Zheng¹, Hao Sun¹, Yingjun Zhao⁵, Yunwu Zhang¹, Maoqiang Xue⁶, Timothy Y. Huang⁵, Guojun Bu⁷, Huaxi Xu⁵, Zengqiang Yuan⁸, Karl Herrup³, Jie Zhang^{1,#}

¹Fujian Provincial Key Laboratory of Neurodegenerative Disease and Aging Research, Institute of Neuroscience, School of Medicine, Xiamen University, Xiamen, Fujian, China.

²School of Life Sciences, The Chinese University of Hong Kong, Sha Tin, Hong Kong

³Department of Neurobiology, School of Medicine, University of Pittsburgh, Pittsburgh, PA, USA

⁴Department of Traditional Chinese Medicine, Medical College, Xiamen University, Xiamen 361102, China

⁵Neuroscience Initiative, Sanford Burnham Prebys Medical Discovery Institute, La Jolla, CA

⁶Department of Basic Medical Science, Medical College, Xiamen University, Xiamen, Fujian, China

⁷Department of Neuroscience, Mayo Clinic, Jacksonville, FL, USA

⁸The Brain Science Center, Beijing Institute of Basic Medical Sciences, Beijing, China

*equal contribution

To whom correspondence should be:

Jie Zhang, Phone/Fax: (86)592-2180717; E-mail: jiezhang@xmu.edu.cn Institute of Neuroscience, School of Medicine, Xiamen University, Xiamen, Fujian 361102, China.

Hei-Man Chow, Phone/Fax: (852)3943-1530/(852)2603-7732; Email: heimanchow@cuhk.edu.hk School of Life Sciences, The Chinese University of Hong Kong, Sha Tin, Hong Kong

Running title: BAG3 modulates synaptic protein turnover

Key words: CDK5, BAG3, HSP70, Synaptic function, Alzheimer's disease, signaling

Abstract

Background

Synaptic protein dyshomeostasis and functional loss is an early invariant feature of Alzheimer's disease (AD), yet the unifying etiological pathway remains largely unknown. Knowing that cyclin-dependent kinase 5 (CDK5) plays critical roles in synaptic formation and degeneration, its phosphorylation targets were re-examined in search for candidates with direct global impacts on synaptic protein dynamics, and the associated regulatory network was also analyzed.

Methods

Quantitative phospho-proteomics and bioinformatics analyses were performed to identify top-ranked candidates. A series of biochemical assays were used to investigate the associated regulatory signaling networks. Histological, electrochemical and behavioral assays were performed in conditional knockout, shRNA-mediated knockdown and AD-related mice models to evaluate its relevance to synaptic homeostasis and functions.

Results

Among candidates with known implications in synaptic modulations, BCL2-associated athanogene-3 (BAG3) ranked the highest. CDK5-mediated phosphorylation on Ser297/Ser291 (Mouse/Human) destabilized BAG3. Loss of BAG3 unleashed the selective protein degradative function of the HSP70 machinery. In neurons, this resulted in enhanced degradation of a number of glutamatergic synaptic proteins. Conditional neuronal knockout of *Bag3 in vivo* led to impairment of learning and memory functions. In human AD and related-mouse models, aberrant CDK5-mediated loss of BAG3 yielded similar effects on synaptic homeostasis. Detrimental effects of BAG3 loss on learning and memory functions were confirmed in these mice, and such were reversed by ectopic BAG3 re-expression.

Conclusions

Our results highlight that neuronal CDK5-BAG3-HSP70 signaling axis plays a critical role in modulating synaptic homeostasis. Dysregulation of the signaling pathway directly contributes to synaptic dysfunction and AD pathogenesis.

Introduction

Synaptic loss is an early invariant feature of Alzheimer's disease (AD), and that a positive relationship exists between the extent of synaptic loss and the severity of dementia (1). Synaptic plasticity—the molecular basis of learning and memory—depends heavily on the physical composition and structure of synapses (2). Changes in synaptic protein dynamics are driven predominantly by the regulation of post-translational modifications, particularly protein phosphorylation (2). CDK5 is an atypical cyclin-dependent kinase that is activated not by traditional cyclins but cyclin-like activators CDK5R1 (p35 and its calpain-cleaved form: p25). Sustained interaction with p25 is believed to activate CDK5 aberrantly, resulting in neurodegeneration (3-5). Elevated p25 level is reported in brain regions afflicted by classic AD pathologies (5, 6). Known as a tau kinase (7), aberrant CDK5 activity contributes to tau hyperphosphorylation and formation of neurofibrillary tangles. CDK5 also phosphorylates and activates β -secretase, thereby promoting β -amyloid and plaque formation (8, 9). Together, inhibition to aberrantly-activated CDK5 is therefore suggested to be a potential disease modulator of AD. However, while some studies support this notion, an increasing amount of evidence indicates that adequate CDK5 activity is important for modulating synaptic function in post-mitotic neurons. For example, *Cdk5r1* knockout mice which confer to dysfunctional CDK5 revealed impairments in long-term depression and formation of spatial learning memories (10). Alternatively, induction of long-term potentiation (LTP) was also found impaired in the neuron-specific *Cdk5*-conditional knockout mouse model (11, 12).

Based on these findings, CDK5 is known as a classic modulator of synaptic plasticity. At the post-synaptic membrane, CDK5 phosphorylates and promotes degradation of N-methyl-D-aspartate (NMDA) receptor subunit NR2B, thereby modulates NMDA receptor complexes and conductance levels (13). Along the dendrites, the kinase also phosphorylates and regulates the stability and abundance of a number of substrates which play crucial roles in the formation (e.g. CRMP1, MEF2) and retraction (e.g. WAVE1, ephexin1) of dendritic spines (2). Thus, CDK5 is deemed to be an important regulator to facilitate synaptic protein turnover. The existing knowledge on known CDK5 substrates suggests that majority of them

are fundamental synaptic components. By considering their changes individually however is insufficient to explain how CDK5 plays a system role in modulating global synaptic protein abundance and homeostasis. In attempt to understand the underlying mechanism, an unbiased Stable Isotope Labeling by Amino acids in Cell culture (SILAC) method was deployed to re-characterize the phospho-regulatory signaling network resulted from CDK5 activation. Among the hits identified, BCL2-associated athanogene-3 (BAG3) was the highest ranked candidate with a propensity to regulate global synaptic protein homeostasis.

Autophagy is an effective degradative pathway that digests cellular components and maintain cellular proteostasis (14). BAG3 is an emerging regulator of autophagy. It functions as a co-chaperone and interacts with heat shock proteins (e.g. HSP70). HSPs involved in either facilitating protein folding or regulating protein degradation by ubiquitin-proteasome system and autophagy pathways (15, 16), depending on the context of interacting co-chaperone (17). Previous studies revealed that BAG3-HSP70 complex favors protein refolding and recycling (18-21); however, when BAG3 was replaced, for instance by BAG1 which contains an ubiquitin-like domain that recruits E3 ligase (e.g. C-terminus of HSC70-Interacting Protein, CHIP(22)), the BAG1-HSP70 complex then favors protein degradation action (23). HSP70-mediated selective protein degradation is an adaptive mechanism in stressed or aging cells for modulating protein homeostasis (24, 25) and in a number of diseases including cancer (26, 27) and neurodegenerative disorders (28).

In agreement with previous findings (29-33), our analyses confirmed that BAG3 localizes in neurites and synaptosomes of mature neurons in the pre-frontal cortex and hippocampal regions. Analyses of BAG3 regulatory network revealed that BAG3 is a novel target of CDK5. CDK5-mediated phosphorylation at S297 residue promotes BAG3 degradation. Loss of BAG3, as a result of aberrant CDK5 activation or by direct gene knockdown, leads to aberrant HSP70(*Hsp1a1*)-mediated degradation of synaptic proteins and neurotransmitter receptors, and hence impairs synaptic plasticity and LTP in neurons. At behavioral level, loss of neuronal BAG3 in the forebrain and hippocampal regions impairs memory- and cognitive-related functions. Using Alzheimer's disease (AD) as a disease model,

reductions of BAG3 were observed in post-mortem brain samples of AD patients and AD-mice. Further investigation using AD mouse models confirmed that BAG3 is a critical modulator of synaptic function in the disease, as deficits in synaptic protein abundance, electrophysiological properties of neurons, and cognitive- and memory-related functions were rescued upon ectopic re-expression of BAG3. Taken together, our findings revealed CDK5-BAG3-HSP70 is a novel signaling axis by which CDK5 commands both the maintenance of normal synaptic function as well as the initiation of synaptic functional decline in pathological aging brain.

Methods and Materials

Antibodies and chemical reagents

Details can be found in *Supplementary materials and methods*. Unless otherwise specified, all reagents were purchased from Sigma.

Animal maintenance, brain tissue harvesting and primary neuronal culture

All animal experiments were approved by and conducted in accordance with the guidelines of the Animal Ethics Committee of Xiamen University and their care was in accord with institutional and regional government guidelines. Details of various mice strains and sources can be found in *Supplementary materials and methods*.

Brain tissue harvesting and neuronal culture experiments were performed as previously described (34), details can be found in *Supplementary materials and methods*.

Post-mortem human brain tissues

Human autopsy tissues from eight individuals diagnosed with AD and eight age-matched controls were obtained from the NICHD Brain and Tissue Bank of Developmental Disorders at the University of Maryland, Baltimore, MD [NICHD Brain Tissue Bank for Developmental Disorders and NICHD (Contract #N01-HD-4-3368 and N01-HD-4-3383)]. Details can be found in *Supplementary materials and methods*.

Other experiments

Details on animal behavioral studies; electrophysiological recordings; western blotting; RT-PCR; immunohistology/immunocytochemistry; expression plasmid and small interference RNA (siRNA) vector construction; adeno-associated virus production and purification; Golgi staining assay; LC-MS/MS and SILAC proteomic analyses; as well as intracranial injection assays can be found in *Supplementary materials and methods*.

Quantitation and statistical analysis

All data were obtained from at least three separate experiments. Statistical analyses of the data were performed using GraphPad Prism 5. All data were presented as the Mean \pm SEM. P values smaller than 0.05 ($P < 0.05$) represent statistical significance.

Results

CDK5-mediated phosphorylation on Ser297/Ser291 (Mouse/Human) promotes BAG3 degradation

To unbiasedly identify potential targets and signaling network of CDK5 which modulate synaptic protein homeostasis, two large-scale, SILAC-based quantitative phospho-proteomics experiments were performed in Neuro2a (N2a) cells harboring different levels of CDK5 activities (Figure 1A). From the unique lists of phospho-peptides enriched in samples with activated CDK5 (Table S1-2), we subsequently refined potential CDK5 candidates through screening candidates with their phosphorylated serine or threonine residues located prior a proline residue (i.e. the canonical p[S/T]P cyclin-dependent kinase (CDK)-targeting motif). From this enrichment, 1,591 of them carried the pSP motifs while 143 of them carried pTP motifs. A further in-depth analysis on the relative distribution of amino acid residues surrounding these phosphorylation sites revealed strong frequencies of arginine (R), histidine (H) and lysine (K) residues at position +3 relative to the phosphorylation sites (Figure 1B), a pattern revealed that these were likely CDK5-specific targets (35, 36). By applying an additional benchmark that allowed only candidates with >1.5 -fold phosphorylation enrichment to be selected, a subset of 215 phospho-peptide fragments belonging to 160 proteins was finally enriched (Figure 1A). Functional characterization of these enriched hits

using the Ingenuity Pathway Analysis (IPA, Qiagen) revealed 50% of them were clustered. Adopting the **Gene Ontology** (GO) biological function as the clustering parameter, majority of the clustered hits played potential roles in neurological disease (Figure 1C). In search for the highest ranked candidate with reported roles in regulating synaptic function and protein homeostasis, BAG3 was identified (Table S1-2) with phosphorylation at S297 residue significantly enriched upon CDK5 activation (Figure 1D).

To validate BAG3 was truly a CDK5 target, we referenced the canonical CDK5 targeting motif [S/T]PX[K/H/R] in which X represents any amino acids and sought for matching amino acid sequence motifs on BAG3 (37, 38). Five well-conserved potential CDK5-targeting serine or threonine residues on BAG3 were identified (Figure 2A). *In vitro* kinase assays performed in human HEK293T cells released that S297 residue was the only CDK5 target, as phosphorylation was completely lost when this residue was mutated into a non-phosphorylatable alanine (Figure 2B). To further investigate the phosphorylation of BAG3 on S297 by CDK5, we generated an antibody raised against phospho-BAG3 (S297). Strong phosphor-signal can be detected in HEK293T cells with ectopic CDK5/P25 expression (Figure 2C). We also harvested brain lysates from Embryonic Day 18 old *Cdk5* knockout mice. Notably, in the absence of CDK5, while phospho-BAG3 level was reduced, yet total BAG3 level revealed a reverse trend (Figure 2D). With gene transcription of *Bag3* in these mice remained unchanged (Figure 2E), this hinted that S297 phosphorylation on BAG3 may modulate its protein stability. In reversely prove the observation, ectopic CDK5 expression resulted in stronger pBAG3-S297 signal yet a drop in total BAG3 was observed in HEK293T cells (Figure 2F). The relevance of CDK5 kinase activity rather than its protein physical properties in inducing such phenomenon was confirmed with a CDK5-specific inhibitor, roscovitine (Figure 2G). To gain a better understanding on how BAG3 protein became downregulated under the influence of CDK5, we modulated protein synthesis and degradation properties of the cells. Treatment of protein synthesis inhibitor cycloheximide (CHX) revealed that the rate of total BAG3 loss was significantly faster in cells with enhanced CDK5 activities (Figure 2H). To determine whether the loss of BAG3 induced by CDK5-p25 was regulated by the proteasome, we used MG132 to inhibit proteasomal activity after CHX treatment. As shown in Figure 2I, the down-regulation of BAG3 by CDK5-p25 shown in

Figure 2H was blocked by MG132. Together, these confirmed that CDK5-mediated phosphorylation on S297 promotes BAG3 protein degradation.

BAG3 modulates glutamatergic synaptic protein turnover through interacting with HSP70

CDK5 is an important regulator of synaptic plasticity, and that BAG3 is an emerging modulator of autophagy, we therefore questioned if BAG3 regulates synaptic protein abundance and function in the brain. During brain development, level of BAG3 but no other family members of BAG (e.g. BAG1 or BAG2) was increased (Figure 3A). The timing of change indeed coincided with the postnatal induction time of multiple synaptic proteins (Figure 3A). Further subcellular fractionation analysis revealed that BAG3 enriched in postsynaptic density fraction (PSD) in DIV21 mature neurons (Figure 3B). This phenomenon was further confirmed by immunocytochemistry analysis (Figure 3C). We hypothesized BAG3 at synaptic region may interact with local synaptic proteins, therefore we analyzed its potential binding partners using LC-MS/MS. In cortical neurons, either overexpressed the GFP-tagged BAG3 or GFP protein, co-immunoprecipitation was performed using an anti-GFP antibody. Subsequent LC-MS/MS analysis revealed 367 hits from lysates with GFP-tagged BAG3, among which 176 hits were commonly identified from lysates with GFP protein. By screening out the common hits, 191 unique potential BAG3 binding partners were identified (Figure 3D, Table S3). GO biological function analysis revealed that they were likely involved in vesicle transport and localization (Figure 3E). Using the alternative Kyoto Encyclopedia of Genes and Genomes (KEGG) clustering criteria, 61 pathways were enriched and among the top 10 pathways were the “Insulin secretion” (Rank 2nd) and Metabolic-related pathways (Rank 3rd to 5th) (TCA cycle; Metabolic Pathways and Carbon metabolism) (Figure 3F) which were known functions of BAG3 (39, 40). More importantly, the same ranking analysis also identified pathways relevant to synaptic function and AD, including “Synaptic vesicle cycle” (Rank 1st); Long-term potential (Rank 8th), and Alzheimer’s disease (Rank 6th) (Figure 3F). Notably, CDK5R1 (p35/p25) was identified among the binding candidates and it belonged to the AD pathway (Figure 3F). A number of presynaptic as well as postsynaptic proteins which play important roles in LTP and AD were also identified (Figure 3F, bottom). These included

the presynaptic SYN1; AMPA receptor subunits GLUR1 and GLUR2; NMDA receptor subunits NR1 and NR2A, and postsynaptic marker PSD95. Their direct interactions with BAG3 were reconfirmed by the *in vitro* GST-pull down analysis from mouse brain lysates using purified GST or GST-Tagged BAG3 harvested from bacteria (Figure 3G). We next hypothesized that the loss of BAG3 upon CDK5-mediated phosphorylation indeed plays a critical role in synaptic dysfunction. Adeno-associated virus (AAV)-mediated *Bag3* knockdown in neurons significantly reduced a number of synaptic proteins, including SYN1, SYP and PSD95 (Figure S1A-C). Subsequently, *in vivo* analyses were performed by stereotactic injection of the AAV into P0 pups (Figure 3H-I). At 90 days after injection, chronic effects of *Bag3* knockdown was evaluated. Although slight reductions in body weights were observed (Figure S1D), significant reductions in synaptic receptor proteins, including GLUR1, GLUR2, NR1 and NR2A were observed in the prefrontal cortex (Figure 3J). Histological Golgi staining was performed, which revealed impaired neuronal arborization and reduced number of dendritic spines in both hippocampal (Figure 3K) and prefrontal cortex (Figure S2A-D) regions in these mice. To further confirm the above observation, neuronal-specific *Bag3* conditional knockout mice (Nestin-Cre/*Bag3*^{fl/fl}) were generated and these mice grow normally (Figure S3A-D). We observed significantly decreasing of BAG3 and synaptic components like GLUR1 and NR1 in both hippocampus and cortex of these animals (Figure S3E-F).

To understand the mechanism behind BAG3 modulation of synaptic protein and receptor abundances, we explored its co-chaperone role in regulating protein homeostasis (41, 42). On the list of BAG3 interacting partners (Table S3), family members of HSP70 including HS12A (*Hspa12a*), HS74L (*Hspa4l*), HSP74 (*Hspa4*) and HSP70/HSP72 (*Hspa1a*) were identified. HSP70/HSP72 (*Hspa1a*) promotes the degradation of target proteins through direct protein-protein interaction (43, 44) and that the presence of BAG3 as a competitor suppresses this mechanism (45, 46). To confirm if HSP70 targets synaptic proteins and share similar interactome as that of BAG3 in neurons, we overexpressed GFP-tagged HSP70/HSP72 (*Hspa1a*) or GFP control in neurons, followed by co-immunoprecipitation assay with anti-GFP antibody and LC-MS/MS analysis. A total of 426 hits were identified from the

GFP-HSP70 pulldown, among which 137 overlapped with those identified from the GFP controls, 289 hits were uniquely found which included BAG3 (Figure 4A, Table S4). Subsequent GO Biological pathway clustering analyses of these enriched hits revealed their potential roles in vesicle-mediated transport and its regulation (Figure 4B). Alternative analysis with KEGG clustering criteria again revealed their roles in synaptic structures (“synaptic vesicle cycle”; “glutamatergic synapse” and “dopaminergic synapse”), functions (“long-term potentiation”) and a number of neuro-pathological conditions (“amphetamine addiction”; “Alzheimer’s disease” and “Huntington’s disease”) (Figure 4C). Together, these confirmed that HSP70 action is important for synaptic modulation in neurons. Using the hits identified, comparative analysis between the 289 and 191 interacting proteins of HSP70 and BAG3, respectively, was performed; and that 68 common interacting partners were identified (Figure 4D, Table S5). Pathway analyses again revealed they were involved in synaptic vesicle structure and transport function and a number of neuropathological conditions. (Figure 4E-F). To evaluate if CDK5-mediated loss of BAG3 consequently unleashes HSP70 for synaptic protein interaction and degradation, we utilized the p35 and p25 ectopic expression system to modulate endogenous CDK5 activities (Figure 4G). With advancing activities of CDK5 from p35- to p25-overexpressing cells, phosphorylated BAG(S297) level increased while total BAG3 decreased (Figure 4G). Interaction between BAG3 and HSP70 was consequently diminished, which the latter revealed enhanced interactions with synaptic components (e.g. GLUR1 and SYN1) even their total levels reduced (Figure 4G). The role of HSP70/HSP72 in aberrant CDK5-activity mediated synaptic protein degradation was further validated by *Hspa1a* knockdown, where aberrant loss of GLUR1 and SYN1 in cells overexpressed p25 was prevented (Figure 4H).

BAG3 is crucial for glutamatergic transmission, long-term potential and memory formation

Based on the findings at both molecular and cellular levels, we then evaluated the electrophysiological properties in neurons. Mice with *Bag3* knockdown in the hippocampus region revealed impairments in input/output function for basal synaptic transmission (Figure 5A). Further investigation of neuronal response to paired-pulse facilitation (PPF) showed

reduction of synaptic facilitation at these synapses (Figure 5B). Glutamatergic neurotransmission also revealed deficits in both frequency and amplitude of AMPA- or NMDA-receptor-mediated mEPSCs and eEPSCs (Figure 5C-D, Figure S4A-B). Consequently, long-term potentiation (LTP) induced by high-frequency stimulation was also impaired (Figure 5E). A similar response was also found in the 2-month old Nestin-Cre/*Bag3*^{fl/fl} conditional knockout mice (Figure S5A). Despite these changes, no differences were observed in gamma-aminobutyric acid (GABA) receptor-mediated mIPSCs and eIPSCs (Figure S4C-G). Together, electrophysiology recording emphasized BAG3 is crucial for maintaining synaptic functions in mature neurons, in particular, glutamatergic transmission mediated by AMPA and NMDA receptors.

To understand how these impairments manifest to deficits in animal behaviors, a battery of behavioral analyses were performed. Using the Morris water maze (MWM) paradigm, mice with *Bag3* knockdown in the hippocampus revealed longer escape latency (Figure 5F) and exploration time at the target quadrant (Figure 5G), and fewer entries and longer initial latency time to the target quadrant (Figure 5H). Similar impairments were also observed in the 2-month old Nestin-Cre/*Bag3*^{fl/fl} mice (Figure S5B-E). By the novel object recognition paradigm, while preference to a familiar object was found to be indifferent, frequencies of novel object exploration was significantly reduced in *Bag3* knockdown mice (Figure 5I). Further analyses with the T-maze and Y-maze alternation paradigms revealed that *Bag3* knockdown impaired working memories (Figure S5F-G). In contrast to these cognitive and memory-related functions, *Bag3* knockdown did not induce any anxiety (evaluated by elevated-plus maze and open-field test); depression (evaluated by forced-swimming test) and locomotor incapability (evaluated by Rotarod test) (Figure S5H-K).

BAG3 level is reduced in Alzheimer's disease (AD) brain and its ectopic expression rescued synaptic and functional deficits in AD-related mouse models

Loss of memory and cognitive abnormalities are among the first symptoms reported in patients suffering from AD (47). At cellular level, aberrant CDK5 activity caused by p25 was previously reported in AD, this phenomenon could be induced by incubating primary neurons

with a mix of fibrillated and oligomeric amyloid- β ($A\beta_{1-42}$) over a 6-hour time course (Figure 6A). Phosphorylated BAG3 at S297 and total BAG3 levels again revealed an opposite trend of progression along the treatment time, in which the changes were prevented when sufficient amount of *Cdk5* was knockdown (Figure 6B). The effect of accumulation of humanized amyloid- β on BAG3 was also revealed in brain lysates of PS1/APP (Figure 6C-D) and 5XFAD AD-mouse models (Figure S6A). Extending this to human, total BAG3 was significantly reduced in post-mortem human AD brain samples, particularly in neurons (Figure 6E-F). To test whether BAG3 expression could rescue synaptic deficits and impaired learning and memory defects in AD mice, we specifically generated an AAV construct in which BAG3 is expressed using a CMV promoter (AAV-BAG3) (Figure 7A). We next injected AAV-BAG3 or an AAV-GFP control into hippocampus of 5XFAD mice to specifically restore BAG3 expression *in vivo* (Figure 7A-B). Western blotting analysis revealed that ectopic expression of BAG3 restored levels of GLUR1, SYN1, SNAP25 and SYP, which was likely a result of reduced interaction with HSP70 (Figure S6B-C). Next, we found that BAG3 ectopic expression rescued escape latency deficits during training and improved time spent in the target quadrant in Morris water maze tests (Figure 7C-D). Additionally, LTP deficits observed in 5XFAD mice were also restored by AAV-BAG3 expression (Figure 7E).

Discussion

In this report, we showed that BAG3 is a CDK5 target with crucial roles in modulating synaptic protein turnover. CDK5-mediated phosphorylation on S297 triggers protein degradation of BAG3. Reduced BAG3 unleashes HSP70, results in aberrant interaction and degradation of multiple synaptic proteins in neurons. At cellular level, BAG3 loss selectively reduces glutamatergic synaptic proteins, neurite complexity and synaptic pruning, which subsequently impairs glutamatergic firing, LTP and hippocampal-dependent memory and cognitive functions. Dysregulation of BAG3 also contribute to synaptic dysfunction during AD pathogenesis. In AD-mouse model, BAG3 re-expression reduced synaptic deficits, electrophysiological and behavioral levels. Our study identifies a new CDK5 phosphorylation target and a regulatory mechanism which explain how the kinase systematically modulates

synaptic protein homeostasis and neurotransmission (Figure S7).

As a regulator of autophagy, BAG3 integrates into the cellular chaperone network in which competition and cooperation among different co-chaperones governs the formation of functionally distinct chaperone complexes (48-50). With reference to the reciprocal relationship between BAG1 and BAG3 expression levels during the process of cellular aging, as well as its uniqueness in utilizing HSP70 chaperones in the autophagy pathway found in other cellular system (25), we report here that this mechanism is in play in during neuronal maturation. In mature neurons, reduced BAG3 results in impairment of synaptic abundance function, inducing deficits in cognitive and memory functions. A recent report revealed that selective BAG3 reduction in excitatory neurons exacerbated tau accumulation, contributing to cellular vulnerability to tau pathology (51). Indeed, our data echo with their findings from different perspectives. We identified BAG3 is a novel target of CDK5, a classic tau kinase. Aberrant CDK5 activity downregulates BAG3, which the activated kinase also introduces tau hyperphosphorylation. On the other hand, our data revealed that BAG3-HSP70 machinery selectively interacts and targets glutamatergic synaptic proteins. Loss of BAG3 leads to aberrant loss of these synapses and functions, resulting in cognitive and memory impairment in mice. Aberrant ubiquitination and degradation of glutamatergic synaptic proteins are reported in contributing to the pathogenesis of AD (52-54). We speculated that if the reciprocal relationship between BAG1 and BAG3 on regulating HSP70 function exists in mature neurons, loss of BAG3 would favor BAG1-HSP70 interaction, hence promoting E3 ligase-dependent proteasome degradation of glutamatergic synaptic proteins (55). It would be interesting to know as well if the action of HSP70 machinery is involved BAG3 effect on tau accumulation (51), and these details warrant future investigation.

The maintenance of healthy synapses keeps a delicate balance between synaptic protein synthesis and degradation (56). While many reports attribute the loss of synaptic function to reduced biosynthesis of these proteins (57-59), here we provide evidence to support an alternative mechanism which reduction of synaptic proteins could be a result of aberrant HSP70-mediated degradation in conditions where BAG3 was lost. In the nervous system,

HSP70 family members are induced in response to injuries and stress conditions like stroke, epilepsy or trauma (60). Depending on the cellular context and conditions, enhanced expression of HSP70 can be either neuroprotective or neurotoxic (60-62). For example, pharmacological induction of HSP70 in a mouse model of amyotrophic lateral sclerosis resulted in caspase-mediated apoptosis of motor neurons (63); while mixed effects of HSP70 function were observed in a kainic acid (KA)-induced epilepsy model (62, 64). We propose that such inconsistencies indicated that complex regulatory mechanisms exist in modulating HSP70 actions. Here we show that CDK5-BAG3-HSP70 signaling axis is one of these examples. CDK5 is an important regulator of different synaptic proteins and neurotransmitter receptors (65-69).

Here we propose a novel mechanism by which CDK5 modulates synaptic function in a systematic manner—by regulating the BAG3-HSP70 autophagy network. Although our data ascribed a neurotoxic outcome to the activation of CDK5, it is important to recall that timing and duration is an important facet of this phenomenon. This is so because transient CDK5 activation is not pathological, but rather an essential part of synaptic plasticity and the formation of hippocampus-dependent memory (70). Our findings are the first to link the chronic activation of CDK5 with the previously unrecognized BAG3-HSP70 relationship, further supporting our model of synaptic protein modulation. By regulating the strength and duration of BAG3-HSP70 interaction, CDK5 activity coordinates the turnover of glutamatergic synaptic proteins and maintains their concentrations within the appropriate range. The balance between synaptic protein synthesis and degradation is needed for late LTP to occur, as co-application of protein degradation blockers and translational inhibitors is able to restore late LTP, which is otherwise blocked when these inhibitors are applied separately (71). Our finding again explains the dynamic effect CDK5 has on synaptic strength and circuit dynamics in the nervous system. With strategies like pharmacological intervention against CDK5 activity being proposed for AD and other neuropathological conditions (72). It is important to remember that either a chronic blockade of activity or a sustained gain of function would both disrupt the normal BAG3-HSP70 dynamics. Going forward, it will be important to study whether there are compartment-specific characteristics of the synthesis and degradation machinery and how these events are exactly coordinated in the future.

Acknowledgements

We acknowledge the generosity of many different laboratories in providing majority of the DNA vectors utilized in this study. We also thank the BrainVTA company for generating AAV particles. This work was supported by the National Science Foundation in China (Grant: 31571055, 81522016, 81271421 to J.Z.; 81801337 to L.L.; 81774377 and 81373999 to L.W.); Fundamental Research Funds for the Central Universities of China-Xiamen University (Grant: 20720150062, 20720180049 and 20720160075 to J.Z.); Fundamental Research Funds for Fujian Province University Leading Talents (Grant JAT170003 to L.L.); Hong Kong Research Grants Council (HKUST12/CRF/13G, GRF660813, GRF16101315, AoE/M-05/12 to K.H.; GRF16103317, GRF16100718 and GRF16100219 to H.-M,C.); Offices of Provost, VPRG and Dean of Science, HKUST (VPRGO12SC02 to K.H.); Chinese University of Hong Kong (CUHK) Improvement on Competitiveness in Hiring New Faculty Funding Scheme (Ref. 133), CUHK Faculty Startup Fund and Alzheimer's Association Research Fellowship (AARF-17-531566) to H.-M, C.

Author Contributions

J.C.Z, H.-M,C., and J.Z. conceptualized the study. H.-M,C., Y.H.G, K.Z. designed and performed morphological analysis and biochemical assays. Y.H.G., G.M.C., J.C.Z., J.Y.L., and M.S. performed behavior tests. D.W. performed pre-experiments. J.C.Z., J.Y.L., M.S., and K.Z. performed the AAV virus injection. J.C.Z., J.Y.L., M.S., H.L., L.G.L., Y.H., D.W., W.T.X. prepared and maintained the mice in Xiamen; H.-M,C. did the same in Hong Kong. Y.L., Y.H.G., N.Z.Z., and M.D.W. performed electrophysiology experiments and Golgi staining. L.W. and H.S. supervised the electrophysiology experiments. G.M.C. and H.F.L. performed the primary neuronal culture. H.-M,C., K.H., and J.Z. wrote the manuscript. Y.W.Z., Z.Q.Y., Y.J.Z., T.Y.H., H.X., and G.B. discussed and edited the manuscript. J. Z. supervised the project.

Conflict of interest

The authors report no biomedical financial interests or potential conflicts of interest.

REFERENCES

1. Shankar GM, Walsh DM (2009): Alzheimer's disease: synaptic dysfunction and Abeta. *Mol Neurodegener.* 4:48.
2. Lai KO, Ip NY (2009): Recent advances in understanding the roles of Cdk5 in synaptic plasticity. *Biochim Biophys Acta.* 1792:741-745.
3. Cruz JC, Tseng HC, Goldman JA, Shih H, Tsai LH (2003): Aberrant Cdk5 activation by p25 triggers pathological events leading to neurodegeneration and neurofibrillary tangles. *Neuron.* 40:471-483.
4. Hamdane M, Buee L (2007): The complex p25/Cdk5 kinase in neurofibrillary degeneration and neuronal death: the missing link to cell cycle. *Biotechnol J.* 2:967-977.
5. Patrick GN, Zukerberg L, Nikolic M, de la Monte S, Dikkes P, Tsai LH (1999): Conversion of p35 to p25 deregulates Cdk5 activity and promotes neurodegeneration. *Nature.* 402:615-622.
6. Tseng HC, Zhou Y, Shen Y, Tsai LH (2002): A survey of Cdk5 activator p35 and p25 levels in Alzheimer's disease brains. *FEBS Lett.* 523:58-62.
7. Piedrahita D, Hernandez I, Lopez-Tobon A, Fedorov D, Obara B, Manjunath BS, et al. (2010): Silencing of CDK5 reduces neurofibrillary tangles in transgenic alzheimer's mice. *J Neurosci.* 30:13966-13976.
8. Song WJ, Son MY, Lee HW, Seo H, Kim JH, Chung SH (2015): Enhancement of BACE1 Activity by p25/Cdk5-Mediated Phosphorylation in Alzheimer's Disease. *PLoS One.* 10:e0136950.
9. Giusti-Rodriguez P, Gao J, Graff J, Rei D, Soda T, Tsai LH (2011): Synaptic deficits are rescued in the p25/Cdk5 model of neurodegeneration by the reduction of beta-secretase (BACE1). *J Neurosci.* 31:15751-15756.
10. Ohshima T, Ogura H, Tomizawa K, Hayashi K, Suzuki H, Saito T, et al. (2005): Impairment of hippocampal long-term depression and defective spatial learning and memory in p35 mice. *J Neurochem.* 94:917-925.
11. Wei FY, Tomizawa K, Ohshima T, Asada A, Saito T, Nguyen C, et al. (2005): Control of cyclin-dependent kinase 5 (Cdk5) activity by glutamatergic regulation of p35 stability. *J Neurochem.* 93:502-512.
12. Hawasli AH, Benavides DR, Nguyen C, Kansy JW, Hayashi K, Chambon P, et al. (2007): Cyclin-dependent kinase 5 governs learning and synaptic plasticity via control of NMDAR degradation. *Nat Neurosci.* 10:880-886.
13. Plattner F, Hernandez A, Kistler TM, Pozo K, Zhong P, Yuen EY, et al. (2014): Memory enhancement by targeting Cdk5 regulation of NR2B. *Neuron.* 81:1070-1083.
14. Liang Y (2019): Emerging Concepts and Functions of Autophagy as a Regulator of Synaptic Components and Plasticity. *Cells.* 8.
15. Takayama S, Reed JC (2001): Molecular chaperone targeting and regulation by BAG family proteins. *Nat Cell Biol.* 3:E237-241.
16. Penke B, Bogar F, Crul T, Santha M, Toth ME, Vigh L (2018): Heat Shock Proteins and Autophagy Pathways in Neuroprotection: from Molecular Bases to Pharmacological Interventions. *Int J Mol Sci.* 19.
17. Lanneau D, Wettstein G, Bonniaud P, Garrido C (2010): Heat shock proteins: cell protection through protein triage. *ScientificWorldJournal.* 10:1543-1552.
18. Rosati A, Ammirante M, Gentilella A, Basile A, Festa M, Pascale M, et al. (2007): Apoptosis

inhibition in cancer cells: a novel molecular pathway that involves BAG3 protein. *Int J Biochem Cell Biol.* 39:1337-1342.

19. Coulson M, Robert S, Saint R (2005): *Drosophila* starvin encodes a tissue-specific BAG-domain protein required for larval food uptake. *Genetics.* 171:1799-1812.
20. Gentilella A, Passiatore G, Deshmane S, Turco MC, Khalili K (2008): Activation of BAG3 by Egr-1 in response to FGF-2 in neuroblastoma cells. *Oncogene.* 27:5011-5018.
21. Du ZX, Meng X, Zhang HY, Guan Y, Wang HQ (2008): Caspase-dependent cleavage of BAG3 in proteasome inhibitors-induced apoptosis in thyroid cancer cells. *Biochem Biophys Res Commun.* 369:894-898.
22. Murata S, Minami Y, Minami M, Chiba T, Tanaka K (2001): CHIP is a chaperone-dependent E3 ligase that ubiquitylates unfolded protein. *EMBO Rep.* 2:1133-1138.
23. Luders J, Demand J, Hohfeld J (2000): The ubiquitin-related BAG-1 provides a link between the molecular chaperones Hsc70/Hsp70 and the proteasome. *J Biol Chem.* 275:4613-4617.
24. Behl C (2016): Breaking BAG: The Co-Chaperone BAG3 in Health and Disease. *Trends Pharmacol Sci.* 37:672-688.
25. Behl C (2011): BAG3 and friends: co-chaperones in selective autophagy during aging and disease. *Autophagy.* 7:795-798.
26. Colvin TA, Gabai VL, Gong J, Calderwood SK, Li H, Gummuluru S, et al. (2014): Hsp70-Bag3 interactions regulate cancer-related signaling networks. *Cancer Res.* 74:4731-4740.
27. Chen J, Zang YS, Xiu Q (2014): BAT3 rs1052486 and rs3117582 polymorphisms are associated with lung cancer risk: a meta-analysis. *Tumour Biol.* 35:9855-9858.
28. Saresella M, Piancone F, Marventano I, La Rosa F, Tortorella P, Caputo D, et al. (2014): A role for the TIM-3/GAL-9/BAT3 pathway in determining the clinical phenotype of multiple sclerosis. *FASEB J.* 28:5000-5009.
29. Choi JS, Lee JH, Kim HY, Chun MH, Chung JW, Lee MY (2006): Developmental expression of Bis protein in the cerebral cortex and hippocampus of rats. *Brain Res.* 1092:69-78.
30. Choi JS, Lee JH, Shin YJ, Lee JY, Yun H, Chun MH, et al. (2009): Transient expression of Bis protein in midline radial glia in developing rat brainstem and spinal cord. *Cell and tissue research.* 337:27-36.
31. Bruno AP, De Simone FI, Iorio V, De Marco M, Khalili K, Sariyer IK, et al. (2014): HIV-1 Tat protein induces glial cell autophagy through enhancement of BAG3 protein levels. *Cell Cycle.* 13:3640-3644.
32. Bruno AP, Festa M, Dal Piaz F, Rosati A, Turco MC, Giuditta A, et al. (2008): Identification of a synaptosome-associated form of BAG3 protein. *Cell Cycle.* 7:3104-3105.
33. Santoro A, Nicolin V, Florenzano F, Rosati A, Capunzo M, Nori SL (2017): BAG3 is involved in neuronal differentiation and migration. *Cell Tissue Res.* 368:249-258.
34. Chow HM, Guo D, Zhou JC, Zhang GY, Li HF, Herrup K, et al. (2014): CDK5 activator protein p25 preferentially binds and activates GSK3beta. *Proc Natl Acad Sci U S A.* 111:E4887-4895.
35. Brown NR, Noble ME, Endicott JA, Johnson LN (1999): The structural basis for specificity of substrate and recruitment peptides for cyclin-dependent kinases. *Nat Cell Biol.* 1:438-443.
36. Shetty KT, Link WT, Pant HC (1993): cdc2-like kinase from rat spinal cord specifically phosphorylates KSPXK motifs in neurofilament proteins: isolation and characterization. *Proc Natl Acad Sci U S A.* 90:6844-6848.
37. Songyang Z, Lu KP, Kwon YT, Tsai LH, Filhol O, Cochet C, et al. (1996): A structural basis for substrate specificities of protein Ser/Thr kinases: primary sequence preference of casein kinases I and II, NIMA, phosphorylase kinase, calmodulin-dependent kinase II, CDK5, and Erk1. *Mol Cell Biol.*

16:6486-6493.

38. Moreno S, Nurse P (1990): Substrates for p34cdc2: in vivo veritas? *Cell*. 61:549-551.
39. An MX, Li S, Yao HB, Li C, Wang JM, Sun J, et al. (2017): BAG3 directly stabilizes Hexokinase 2 mRNA and promotes aerobic glycolysis in pancreatic cancer cells. *J Cell Biol*. 216:4091-4105.
40. Iorio V, Festa M, Rosati A, Hahne M, Tiberti C, Capunzo M, et al. (2015): BAG3 regulates formation of the SNARE complex and insulin secretion. *Cell Death Dis*. 6:e1684.
41. Rosati A, Graziano V, De Laurenzi V, Pascale M, Turco MC (2011): BAG3: a multifaceted protein that regulates major cell pathways. *Cell Death Dis*. 2:e141.
42. Fernandez-Fernandez MR, Valpuesta JM (2018): Hsp70 chaperone: a master player in protein homeostasis. *F1000Res*. 7.
43. Quintana-Gallardo L, Martin-Benito J, Marcilla M, Espadas G, Sabido E, Valpuesta JM (2019): The cochaperone CHIP marks Hsp70- and Hsp90-bound substrates for degradation through a very flexible mechanism. *Sci Rep*. 9:5102.
44. Mayer MP, Gierasch LM (2019): Recent advances in the structural and mechanistic aspects of Hsp70 molecular chaperones. *J Biol Chem*. 294:2085-2097.
45. Kampinga HH, Craig EA (2010): The HSP70 chaperone machinery: J proteins as drivers of functional specificity. *Nat Rev Mol Cell Biol*. 11:579-592.
46. Meister-Broekema M, Freilich R, Jagadeesan C, Rauch JN, Bengoechea R, Motley WW, et al. (2018): Myopathy associated BAG3 mutations lead to protein aggregation by stalling Hsp70 networks. *Nat Commun*. 9:5342.
47. Jahn H (2013): Memory loss in Alzheimer's disease. *Dialogues in clinical neuroscience*. 15:445-454.
48. Alberti S, Bohse K, Arndt V, Schmitz A, Hohfeld J (2004): The cochaperone HspBP1 inhibits the CHIP ubiquitin ligase and stimulates the maturation of the cystic fibrosis transmembrane conductance regulator. *Mol Biol Cell*. 15:4003-4010.
49. Fontanella B, Birolo L, Infusini G, Cirulli C, Marzullo L, Pucci P, et al. (2010): The co-chaperone BAG3 interacts with the cytosolic chaperonin CCT: new hints for actin folding. *Int J Biochem Cell Biol*. 42:641-650.
50. Klimek C, Kathage B, Wordehoff J, Hohfeld J (2017): BAG3-mediated proteostasis at a glance. *J Cell Sci*. 130:2781-2788.
51. Fu H, Possenti A, Freer R, Nakano Y, Hernandez Villegas NC, Tang M, et al. (2019): A tau homeostasis signature is linked with the cellular and regional vulnerability of excitatory neurons to tau pathology. *Nature neuroscience*. 22:47-56.
52. Widagdo J, Guntupalli S, Jang SE, Anggono V (2017): Regulation of AMPA Receptor Trafficking by Protein Ubiquitination. *Front Mol Neurosci*. 10:347.
53. Rodrigues EM, Scudder SL, Goo MS, Patrick GN (2016): Abeta-Induced Synaptic Alterations Require the E3 Ubiquitin Ligase Nedd4-1. *J Neurosci*. 36:1590-1595.
54. Guntupalli S, Jang SE, Zhu T, Hugarir RL, Widagdo J, Anggono V (2017): GluA1 subunit ubiquitination mediates amyloid-beta-induced loss of surface alpha-amino-3-hydroxy-5-methyl-4-isoxazolepropionic acid (AMPA) receptors. *J Biol Chem*. 292:8186-8194.
55. Hantouche C, Williamson B, Valinsky WC, Solomon J, Shrier A, Young JC (2017): Bag1 Co-chaperone Promotes TRC8 E3 Ligase-dependent Degradation of Misfolded Human Ether a Go-Go-related Gene (hERG) Potassium Channels. *J Biol Chem*. 292:2287-2300.

56. Alvarez-Castelao B, Schuman EM (2015): The Regulation of Synaptic Protein Turnover. *J Biol Chem.* 290:28623-28630.
57. Reddy PH, Mani G, Park BS, Jacques J, Murdoch G, Whetsell W, Jr., et al. (2005): Differential loss of synaptic proteins in Alzheimer's disease: implications for synaptic dysfunction. *Journal of Alzheimer's disease : JAD.* 7:103-117; discussion 173-180.
58. Scheetz AJ, Nairn AC, Constantine-Paton M (2000): NMDA receptor-mediated control of protein synthesis at developing synapses. *Nat Neurosci.* 3:211-216.
59. Adachi N, Numakawa T, Kumamaru E, Itami C, Chiba S, Iijima Y, et al. (2013): Phencyclidine-induced decrease of synaptic connectivity via inhibition of BDNF secretion in cultured cortical neurons. *Cereb Cortex.* 23:847-858.
60. Turturici G, Sconzo G, Geraci F (2011): Hsp70 and its molecular role in nervous system diseases. *Biochem Res Int.* 2011:618127.
61. Yang YL, Lin MT (1999): Heat shock protein expression protects against cerebral ischemia and monoamine overload in rat heatstroke. *Am J Physiol.* 276:H1961-1967.
62. Yang T, Hsu C, Liao W, Chuang JS (2008): Heat shock protein 70 expression in epilepsy suggests stress rather than protection. *Acta Neuropathol.* 115:219-230.
63. Kalmar B, Greensmith L (2009): Activation of the heat shock response in a primary cellular model of motoneuron neurodegeneration-evidence for neuroprotective and neurotoxic effects. *Cell Mol Biol Lett.* 14:319-335.
64. Vass K, Berger ML, Nowak TS, Jr., Welch WJ, Lassmann H (1989): Induction of stress protein HSP70 in nerve cells after status epilepticus in the rat. *Neurosci Lett.* 100:259-264.
65. Fletcher AI, Shuang R, Giovannucci DR, Zhang L, Bittner MA, Stuenkel EL (1999): Regulation of exocytosis by cyclin-dependent kinase 5 via phosphorylation of Munc18. *J Biol Chem.* 274:4027-4035.
66. Tomizawa K, Ohta J, Matsushita M, Moriwaki A, Li ST, Takei K, et al. (2002): Cdk5/p35 regulates neurotransmitter release through phosphorylation and downregulation of P/Q-type voltage-dependent calcium channel activity. *J Neurosci.* 22:2590-2597.
67. Shuang R, Zhang L, Fletcher A, Groblewski GE, Pevsner J, Stuenkel EL (1998): Regulation of Munc-18/syntaxin 1A interaction by cyclin-dependent kinase 5 in nerve endings. *J Biol Chem.* 273:4957-4966.
68. Morabito MA, Sheng M, Tsai LH (2004): Cyclin-dependent kinase 5 phosphorylates the N-terminal domain of the postsynaptic density protein PSD-95 in neurons. *J Neurosci.* 24:865-876.
69. Kesavapany S, Lau KF, McLoughlin DM, Brownlees J, Ackerley S, Leigh PN, et al. (2001): p35/cdk5 binds and phosphorylates beta-catenin and regulates beta-catenin/presenilin-1 interaction. *Eur J Neurosci.* 13:241-247.
70. Fischer A, Sananbenesi F, Pang PT, Lu B, Tsai LH (2005): Opposing roles of transient and prolonged expression of p25 in synaptic plasticity and hippocampus-dependent memory. *Neuron.* 48:825-838.
71. Fonseca R, Vabulas RM, Hartl FU, Bonhoeffer T, Nagerl UV (2006): A balance of protein synthesis and proteasome-dependent degradation determines the maintenance of LTP. *Neuron.* 52:239-245.
72. Mushtaq G, Greig NH, Anwar F, Al-Abbasi FA, Zamzami MA, Al-Talhi HA, et al. (2016): Neuroprotective Mechanisms Mediated by CDK5 Inhibition. *Curr Pharm Des.* 22:527-534.

Figure Legends:

Figure 1. Stable isotope labelling by amino acids in cell culture (SILAC) analysis for CDK5 phospho-proteome. (A) Schematic diagram of the experimental flow of SILAC experiment. Bottom plots indicate the ratio distribution of phospho-peptides identified in each set of screening. (B) Binomial distribution of amino acids at positions flanking or lagging the CDK5-targeting serine (S) or threonine (T) residues in enriched ($\log_2 H/L > 1.5$ or 2) phosphor-peptides identified from the SILAC experiments. (C) Ingenuity pathway analysis was performed using the GO Biological Function paradigm. The top 10 enriched pathways are shown. (D) Mass spectrometry profiles of the p35 or the CDK5/p35 SILAC screens reveal BAG3 phosphorylation at Serine 297 residue (S297) was commonly enriched. Unless otherwise specified, all experiments were performed with at least 3 biological repeats; each individual assay was performed at least three times.

Figure 2. CDK5-mediated phosphorylation on S297 promotes BAG3 degradation. (A) BAG3 protein sequences of multiple species were aligned using the Clustal Omega platform. Conserved S/TP sites were highlighted in red. (B) Representative blots of *in vitro* CDK5 kinase assays. Phosphorylation on the recombinant GST-tagged BAG3 mutant proteins was tested *in vitro* in the presence of active CDK5/p35 complex. Reaction products were immunoblotted with CDK5 target specific p[S/T]P antibody. Coomassie blue staining indicates equal loading. (C) Representative blots showing signals of S297 phosphorylation [pBAG(S297)] on V5-tagged BAG3 are present only when GFP-tagged CDK5 and p25 were co-expressed in HEK293T cells. (D) Representative blots showing changes in pBAG3(S297) and BAG3 in response to CDK5 level in Embryonic 18 Day *Cdk5* wildtype, heterozygous and homozygous knockout mice. Both frontal cortex and hippocampal tissues were analyzed. Quantifications are shown on the right (N=6). (E) Quantitative PCR of *Bag3* gene expression in both cortex and hippocampal tissues harvested from wildtype, heterozygous and homozygous *Cdk5* knockout mice (N=6). (F) Representative blots showing changes in pBAG3(S297) and BAG3 levels in accordance with different levels of CDK5 activities in HEK293T cells. Quantifications are shown below (N=6). (G) Representative blots showing changes in pRB, pBAG3(S297) and BAG3 levels in response to pharmacological inhibition of CDK5 by roscovitine for different time courses. Quantifications of band intensity and cellular

CDK5 activity in all treatment time courses are shown. (H) Representative blots showing changes in total BAG3 level in cells of different CDK5 activities subjected to cycloheximide treatment for different time courses. Quantification is shown on the right (N=6). (I) HEK293T cells transfected with GFP-CDK5/p25 were first treated with CHX for 8 hours, and followed 50 μ M MG132 treatment for 2 hours. Representative blots showing changes in total BAG3. Quantification is shown on the right (N=6). Unless otherwise specified, all experiments performed with at least 3 biological repeats, each individual assay was performed at least three times. * $P < 0.05$, ** $P < 0.01$, *** $P < 0.001$, ns=non-significant. Data represent the mean \pm SEM.

Figure 3. BAG3 sustains synaptic protein abundance. (A) Representative blots showing changes of BAG1/2/3, SYN1, NR2A and GLUR1 during neuronal maturation. Quantification is shown (N=6). (B) Representative blots showing enrichments of BAG3 in synaptic fractions enriched from DIV21 primary neurons. Quantification is shown (N=6). (C) Representative immunocytochemistry images showing the distribution of BAG2/3 at synaptic regions of DIV21 primary neurons. Quantification is shown (N=6). (D) Venn diagram shows among the 367 hits identified from GFP-BAG3 pull-down; 176 hits overlapped with those identified from the GFP pull-down using LC-MS/MS analysis (N=6). (E-F) 191 unique GFP-BAG3 interacting partners were clustered using (E) Gene Ontology and (F) KEGG parameters, top 10 enriched pathways are shown. At the bottom of (F) are lists of proteins enriched in corresponding KEGG pathways. (G) *In vitro* pull-down assay of proteins from mouse forebrain lysates using purified GST or GST-Tagged BAG3 harvested from bacteria, was performed. Representative blots showing BAG3 interaction with various synaptic proteins (N=6). (H) Schematic diagram of the structure of the shRNA-BAG3-GFP shuttle and associated workflow in mice. (I) Representative image of AAV-GFP signals in mice reveals viral transduction occurred predominantly in the pre-frontal cortex and hippocampal regions (N=6). (J) Representative blots showing changes in BAG3, pBAG3(S297), GLUR1, GLUR2, NR1, NR2A and CDK5 in cortical tissues harvested from mice received either AAV-Scrambled shRNA or AAV-*Bag3*-shRNA for 90 days. Quantification is shown (N=6). (K) Representative images of Golgi staining of neurite structures and dendritic spines in

hippocampal tissues harvested from mice received either AAV-Scrambled shRNA or AAV-BAG3-shRNA for 30 days. Quantification of spine number is shown (N=6) Unless otherwise specified, all experiments performed with at least 3 biological repeats; each individual assay was performed at least three times. * $P < 0.05$, ** $P < 0.01$, *** $P < 0.001$, ns=non-significant. Data represent the mean \pm SEM.

Figure 4. BAG3 prevents HSP70-synaptic protein interaction hence sustains their abundance. (A). Venn diagram shows among the 426 hits identified from GFP-HSP70 pulldown; 137 hits overlapped with those identified from the GFP pull-down using LC-MS/MS analysis (N=6). (B-C) 289 unique GFP-HSP70 interacting partners were clustered using (B) Gene Ontology and (C) KEGG parameters, top 10 enriched pathways are shown. At the bottom of (C) are lists of proteins enriched in corresponding KEGG pathways. (D) Venn diagram shows 68 common binding partners identified among different set of unique binding partners of BAG3 (Figure 3D) and HSP70. (E-F) 68 common interacting partners were clustered using (E) Gene Ontology and (F) KEGG parameters, top 10 enriched pathways are shown. At the bottom of (F) are lists of proteins enriched in corresponding KEGG pathways. (G) Representative blots showing changes in total levels as well as protein-protein interactions of BAG3, HSP70 and selected synaptic protein levels in neurons ectopically expressed GFP-tagged p35 or p25. Quantification of bands (N=5) as well as corresponding CDK5 activities in different groups are shown (N=9). (H) Representative blots showing changes in total levels as well as protein-protein interactions of BAG3, HSP70 and selected synaptic protein levels in neurons ectopically expressed GFP-tagged p25, together with scrambled siRNA or *Hspa1a* siRNA. Quantification of bands (N=8) as well as corresponding CDK5 activities in different groups are shown (N=9). Unless otherwise specified, all experiments performed with at least 3 biological repeats; each individual assay was performed at least three times. * $P < 0.05$, ** $P < 0.01$, *** $P < 0.001$, ns=non-significant. Data represent the mean \pm SEM.

Figure 5. BAG3 is indispensable for glutamatergic firing, long-term potentiation and memory formation. (A-E) Electrophysiology recordings in brain slices harvested from mice

stereotaxically injected AAV carrying GFP-tagged scrambled shRNA or GFP-tagged *Bag3* shRNA shuttles. Recordings were performed on Day30 post-injection. (A) fEPSP input-output relationship was recorded in hippocampal CA1 region upon stimulation at the superior colliculus region (N=6). (B) Whole-cell eEPSC pair-pause ratio recording pattern recorded in hippocampal CA1 pyramidal neurons (N=6). (C-D) Representative tracing patterns of (C) AMPA receptor- and (D) NMDA receptor-mediated mEPSCs. All recordings were performed at a holding potential of -65mV. Quantitative analyses of corresponding receptor-mediated mEPSC frequencies and amplitudes are shown (N=6). (E) LTP recording in superior colliculus after induction of a train of 100-Hz stimuli. Insets: representative traces of fEPSP responses prior and at 50-min post-high frequency stimulations. Quantitative analyses of fEPSP slopes are shown and the level of fEPSP potentiation was determined by averaging the values between 0 to 3 min and 50 to 60 min post-high frequency stimulations (N=6). (F-H) Morris water maze test was performed in mice stereotaxically injected AAV carrying GFP-tagged scrambled shRNA or GFP-tagged *Bag3* shRNA shuttles. Recordings were performed on Day 90 post-injection. (F) Escape latency trajectory pattern of the initial 6-day training phase is shown (N=6). (G) Time spent in the target zone and other quadrants (NE, SE and SW), as well as (H) the frequency of target zone crossing; and initial time required for reaching the target platform during the probe trial performed on Day7 are shown (N=6). (I) Novel object recognition analysis was performed on Day 90 post-injection. Frequencies of mice accessing familiar (object A) versus novel (object B) objects were recorded. Exploration time was analyzed and shown (N=6). Unless otherwise specified, all experiments performed with at least 3 biological repeats; each individual assay was performed at least three times. * $P < 0.05$, ** $P < 0.01$, *** $P < 0.001$, ns=non-significant. Data represent the mean \pm SEM.

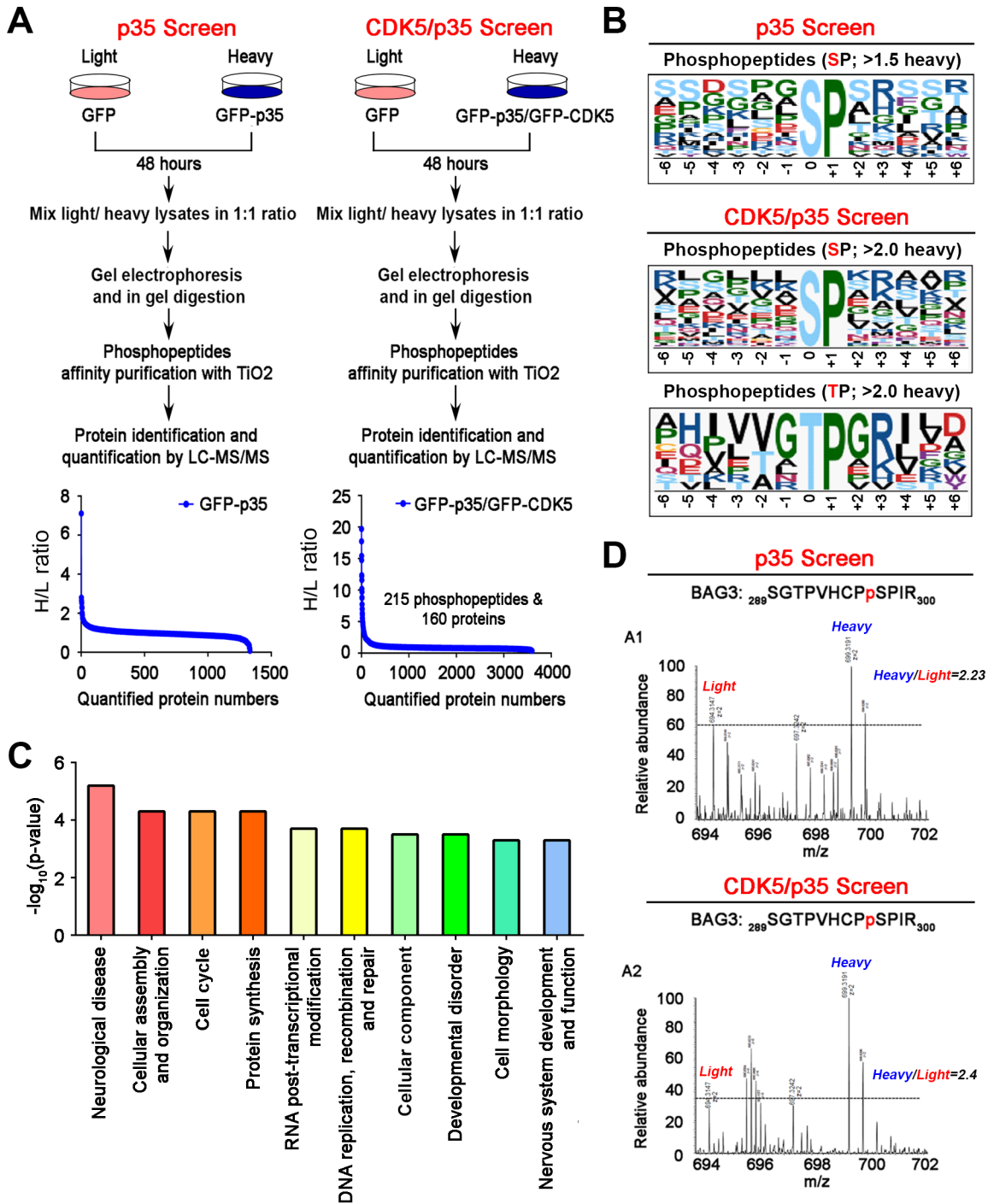
Figure 6. BAG3 is reduced in Alzheimer's disease (AD). (A) Representative blots showing changes in phosphorylated pBAG3(S297), total BAG3, CDK5R1 (p35/p25), CDK5 and HSP70 in neurons exposed a mixture of fibrillated and oligomeric amyloid- β ($A\beta_{1-42}$) peptide for various time courses. Quantification is shown (N=6). (B) Representative blots showing changes in phosphorylated pBAG3(S297), total BAG3, CDK5R1 (p35/p25), CDK5 and HSP70 performed in neurons with or without *Cdk5* knockdown, and exposed a mixture of

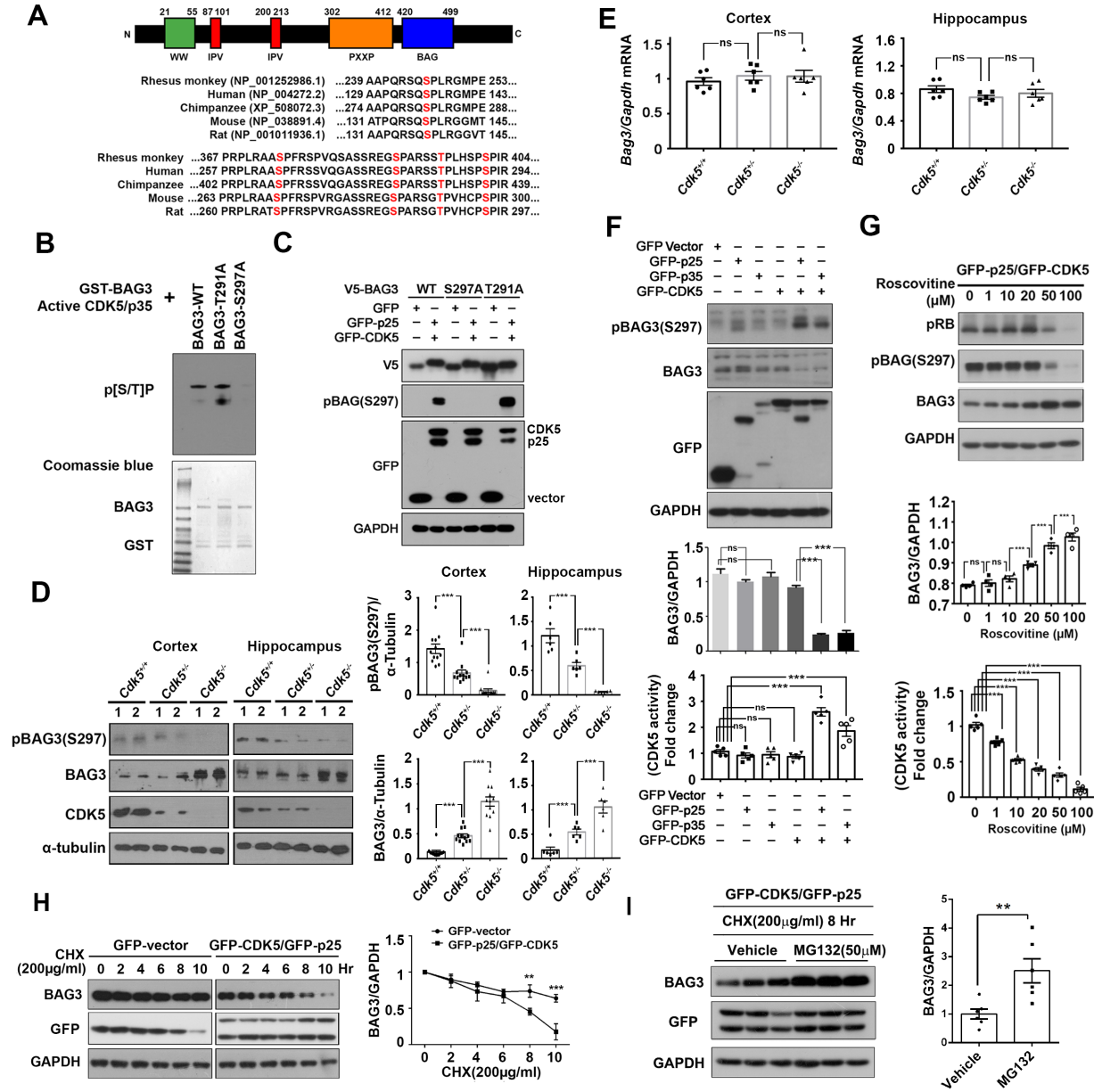
fibrillated and oligomeric amyloid- β ($A\beta_{1-42}$) peptide for 6 hours. Quantification is showed (N=6). (C) Brain cortical samples harvested from 12-month old PS1/APP mice and non-transgenic littermates were analyzed. Representative blots showing differences in phosphorylated pBAG3(S297), total BAG3, CDK5R1 (p35/p25), CDK5 and HSP70 are shown (N=12). Corresponding CDK5 activities (N=6); as well as correlations between (i) pBAG3/GAPDH or (ii) BAG3/GAPDH to p25/GAPDH ratio are shown (N=12). (D) Representative immunohistochemistry images of BAG3 and MAP2 signals in prefrontal cortex regions of PS1/APP mice and littermates are shown (n=10). (E) Post-mortem frozen brain samples from AD patients and non-demented age-matched control were analyzed. Representative blots showing differences in phosphorylated pBAG3(S297), total BAG3, CDK5R1 (p35/p25), CDK5 and HSP70 are shown (N=9); Corresponding CDK5 activities (N=6); as well as correlations between (i) pBAG3/GAPDH or (ii) BAG3/GAPDH to p25/GAPDH ratio are shown (N=9). (F) Representative immunohistochemistry images of BAG3 and MAP2 signals in frontal cortex regions of post-mortem frozen human AD and non-demented age-matched samples (N=9). Unless otherwise specified, all experiments performed with at least 3 biological repeats; each individual assay was performed at least three times. * $P < 0.05$, ** $P < 0.01$, *** $P < 0.001$, ns=non-significant. Data represent the mean \pm SEM.

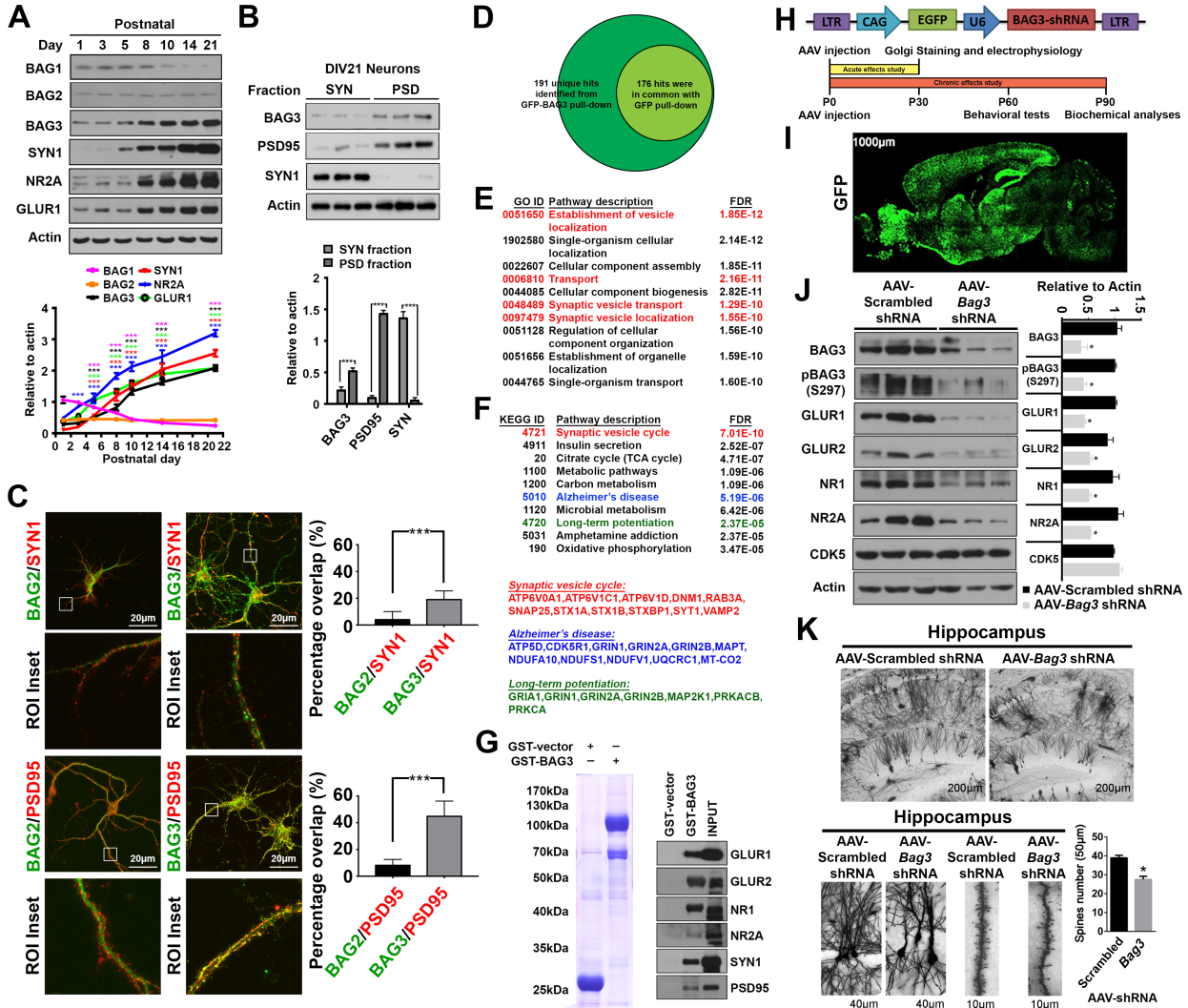
Figure 7. Ectopic expression BAG3 rescued synaptic and functional deficits in 5XFAD AD-mouse model. (A) Schematic diagram shows the construct design for GFP-tagged BAG3, and the experimental workflow. AAV carrying this construct was stereotaxically delivered to hippocampal CA1 region of 4-month old 5XFAD mice. (B) Representative immunohistochemistry images showing GFP-fluorescence and total BAG3 signals in CA1 hippocampal region of 5XFAD mice at 5-weeks post-AAV injections. (C-D) Morris water maze (MWM) test for spatial learning memory was also performed in these mice. (C) The initial latency to target during the 6-day training course was recorded (N=6-7). (D) During the probe trial test on Day 7, the time spent by these mice in the target zone and other quadrants (NE, SE and SW) were recorded (N=6-7). (E) Ectopic expression of BAG3 rescued LTP deficits in hippocampal CA1 region of 5-months old 5XFAD mice. LTP was recorded by

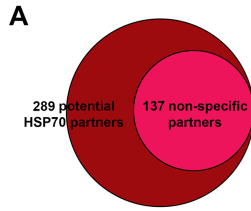
inducing two trains of 100-Hz stimuli at Schaffer Collaterals. A significant difference in fEPSP potentiation was determined by comparing fEPSP slopes during last 10 min of recording after high frequency stimulations (N=6-7). Unless otherwise specified, all experiments performed with at least 3 biological repeats; each individual assay was performed at least three times. * $P < 0.05$, ** $P < 0.01$, *** $P < 0.001$, ns=non-significant. Data represent the mean \pm SEM.

Journal Pre-proof









B

GO ID	Pathway description	FDR
0051641	Cellular localization	3.30E-21
0051128	Regulation of cellular component organization	5.58E-21
0051649	Establishment of localization in cell	1.99E-20
0051234	Establishment of localization	2.15E-20
0006810	Transport	3.88E-20
0016192	Vesicle-mediated transport	3.88E-20
0051179	Localization	3.88E-20
1902578	Single-organism localization	1.35E-19
0051049	Regulation of transport	4.61E-19
0032879	Regulation of localization	4.98E-18

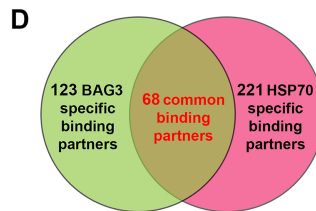
C

KEGG ID	Pathway description	FDR
4721	Synaptic vesicle cycle	1.37E-13
5031	Amphetamine addiction	9.54E-08
4720	Long-term potentiation	1.33E-06
4022	cGMP-PKG signaling pathway	2.20E-06
5010	Alzheimer's disease	2.20E-06
4020	Calcium signaling pathway	3.54E-06
4724	Glutamatergic synapse	5.84E-06
4911	Insulin secretion	6.43E-06
4728	Dopaminergic synapse	1.01E-05
5016	Huntington's disease	1.84E-05

Synaptic vesicle cycle:
AP2A1, ATP6V0A1, ATP6V0D1, ATP6V1H, DNM3, NAPA, NSF, SNAP25, STX1A, STX1B, STXBP1, SYT1, VAMP2

Long-term potentiation:
CAMK2G, GRIA1, GRIN1, GRIN2A, GRIN2B, PPP3CB, PRKCG

Alzheimer's disease:
APOE, ATP2A2, ATP5C1, ATP5F1, GRIN1, GRIN2A, GRIN2B, MAPT, NDUFA12, PPP3CB, MT-CO2



E

GO ID	Pathway description	FDR
0006810	Transport	4.30E-10
0051179	Localization	9.11E-10
1902578	Single-organism localization	4.19E-09
1902580	Single-organism cellular localization	4.85E-09
0044765	Single-organism transport	6.06E-09
0050806	Positive regulation of synaptic transmission	1.57E-08
0016192	Vesicle-mediated transport	2.39E-08
0051049	Regulation of transport	2.75E-08
0007268	Synaptic transmission	1.77E-07
0032879	Regulation of localization	2.89E-07

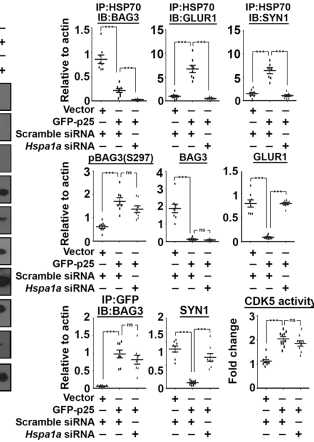
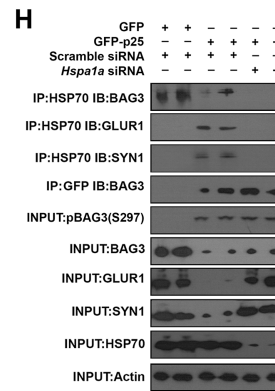
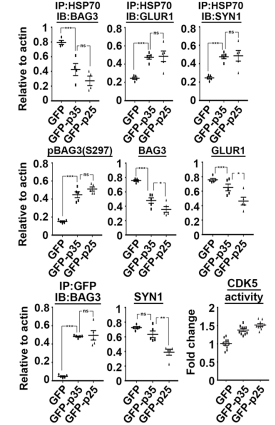
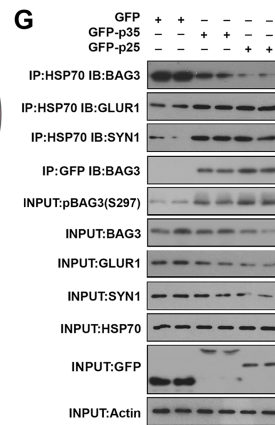
F

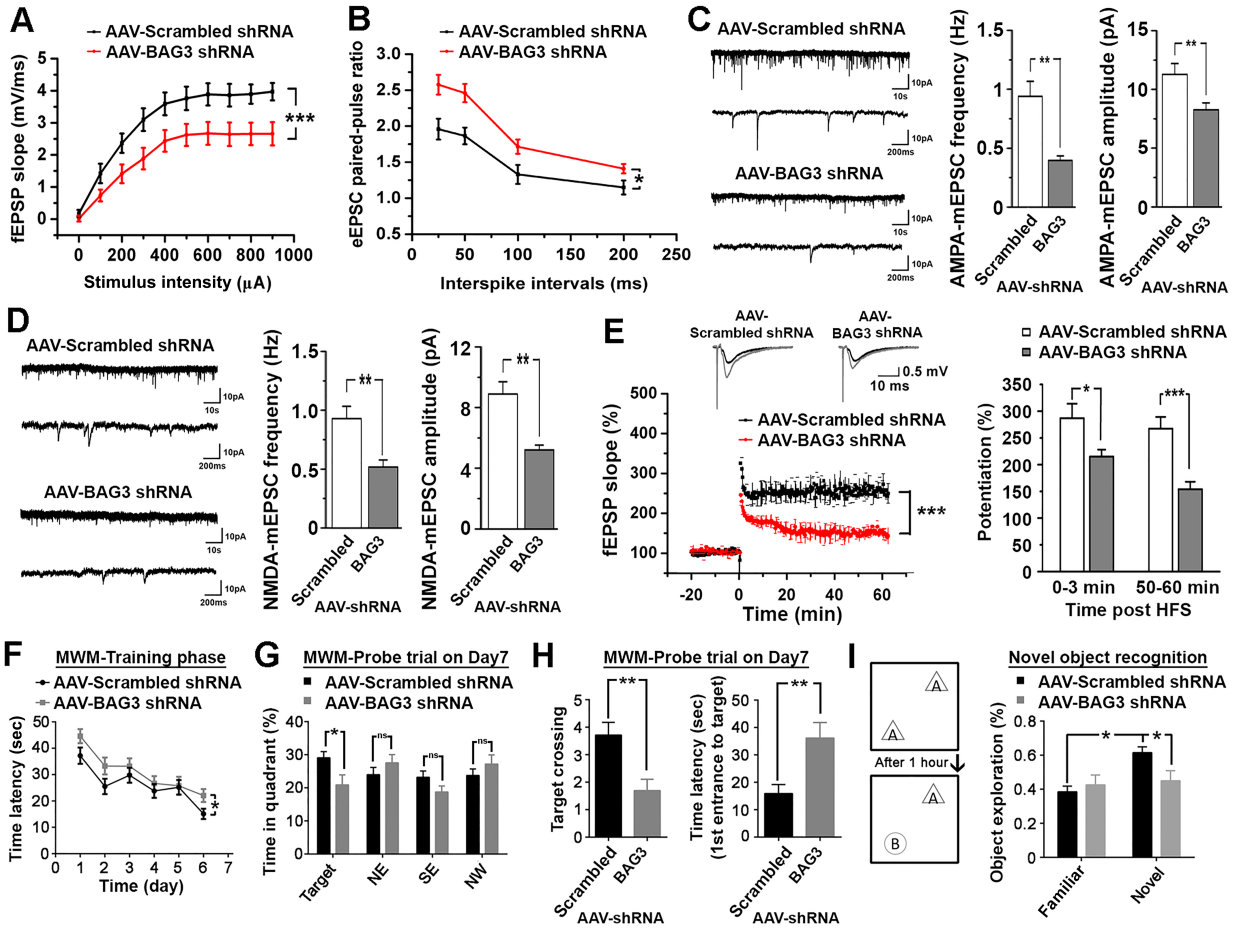
KEGG ID	Pathway description	FDR
4721	Synaptic vesicle cycle	5.10E-09
5031	Amphetamine addiction	1.45E-05
4911	Insulin secretion	4.48E-05
5033	Nicotine addiction	6.29E-05
4724	Glutamatergic synapse	0.000117
5014	Amyotrophic lateral sclerosis	0.000122
4720	Long-term potentiation	0.0002
5010	Alzheimer's disease	0.00044
4713	Circadian entrainment	0.000832
4130	SNARE interactions in vesicular transport	0.000882

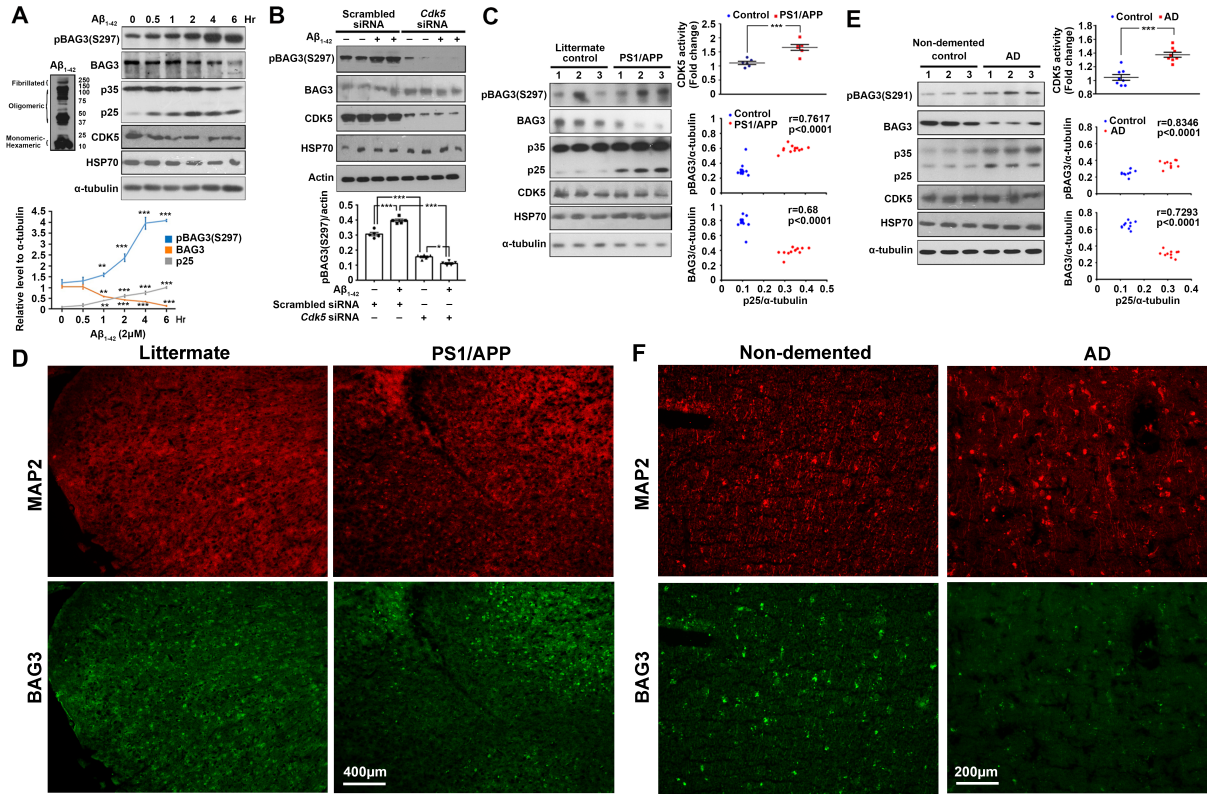
Synaptic vesicle cycle:
ATP6V0A1, SNAP25, STX1A, STX1B, STXBP1, SYT1, VAMP2

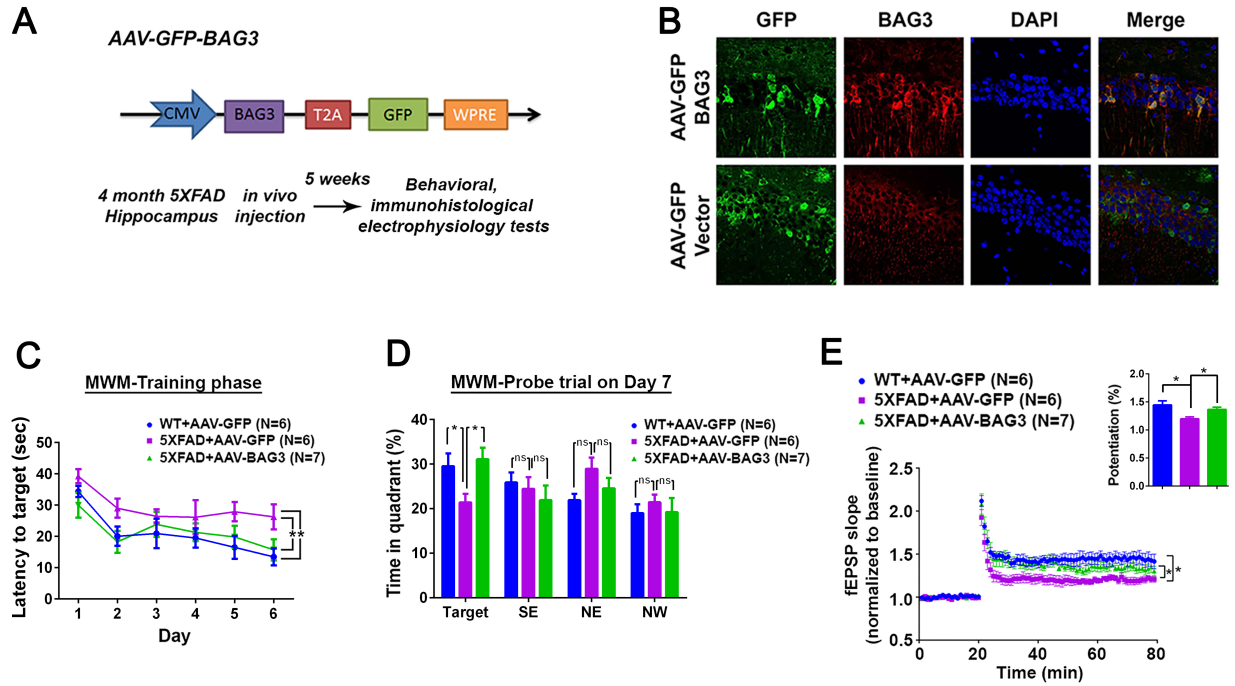
Long-term potentiation:
GRIA1, GRIN1, GRIN2A, GRIN2B

Alzheimer's disease:
GRIN1, GRIN2A, GRIN2B, MAPT, MT-CO2









Resource Type	Specific Reagent or Resource	Source or Reference	Identifiers	Additional Information
Add additional rows as needed for each resource type	Include species and sex when applicable.	Include name of manufacturer, company, repository, individual, or research lab. Include PMID or DOI for references; use "this paper" if new.	Include catalog numbers, stock numbers, database IDs or accession numbers, and/or RRIDs. RRIDs are highly encouraged; search for RRIDs at https://scicrunch.org/resources .	Include any additional information or notes if necessary.
Antibody	Rabbit anti-CDK5	Cell Signaling Technology	2506	
Antibody	Rabbit anti-phospho-CDK Substrate Motif	Cell Signaling Technology	94775	
Antibody	Rabbit anti-pBAG3(S297)	ProSci Incorporated	Custom made	Rabbits were immunized with BAG3 phosphopeptide (PLHSP(pS)PIRVH) to induce immune response. Subsequent serum fractionation with both negative- and positive-affinity purification methods was performed to optimize the specificity for the targeted phosphoepitope
Antibody	Rabbit anti-PSD95	Cell Signaling Technology	3450S	
Antibody	Rabbit anti-cleaved caspase-3	Cell Signaling Technology	9661S	
Antibody	Rabbit anti- β -actin	Cell Signaling Technology	4970S	
Antibody	Rabbit anti-phospho-Rb (Ser807/811)	Cell Signaling Technology	9308S	
Antibody	Rabbit anti-GAPDH	Cell Signaling Technology	5174S	
Antibody	Mouse anti-CDK5	Santa Cruz Biotechnology	sc-6247	
Antibody	Rabbit anti-GFP	Santa Cruz Biotechnology	sc-8334	
Antibody	Rabbit anti-p35 (C-terminal)	Santa Cruz Biotechnology	sc-820	
Antibody	Rabbit anti-p35 (N-terminal)	Santa Cruz Biotechnology	sc-821	
Antibody	Goat anti-V5 probe	Santa Cruz Biotechnology	sc-83849	
Antibody	Mouse anti-GAPDH	Santa Cruz Biotechnology	sc-47724	
Antibody	Mouse anti- α -tubulin	Santa Cruz Biotechnology	sc-8035	
Antibody	Mouse anti- α -tubulin	Sigma Aldrich	T5168	
Antibody	Rabbit anti-Synaptophysin	Sigma Aldrich	SAB4502906	
Antibody	Mouse anti-FLAG	Sigma Aldrich	A2220	
Antibody	Rabbit anti-BAG3	Abcam	ab86298	
Antibody	Goat anti-PSD95	Abcam	ab12093	
Antibody	Rabbit anti-Syntaxin 1	Immunoway	YT5440	
Antibody	Mouse anti-CDK5	Millipore	05-364	
Antibody	Rabbit anti-synapsin 1	Millipore	AB1543	
Antibody	Rabbit anti-NR2A	Millipore	07-632	
Antibody	Mouse anti-GST tag	ProteinTech	HRP-66001	
Antibody	Rabbit anti-GLUR1	Abcam	ab31232	
Antibody	Rabbit anti-GLUR2	Abcam	ab20673	
Antibody	Rabbit anti-NR2B	Abcam	ab65783	
Antibody	Rabbit anti-BAG1	Thermo Fisher	PA5-29585	
Antibody	Rabbit anti-BAG2	Thermo Fisher	PA5-30922	
Antibody	Rabbit anti-BAG3	Thermo Fisher	PA5-54239	
Antibody	Mouse anti-HSP70	Thermo Fisher	MA3-006	
Antibody	Rabbit anti-beta-amyloid	GeneTex	GTX82974	
Antibody	Rabbit anti-APP	GeneTex	GTX101336	
Antibody	Goat anti-mouse ALEXA 488	Thermo Fisher	A28175	
Antibody	Goat anti-mouse ALEXA 594	Thermo Fisher	A-11005	
Antibody	Goat anti-rabbit ALEXA 488	Thermo Fisher	A27034	
Antibody	Goat anti-rabbit ALEXA 594	Thermo Fisher	A-11012	
Bacterial or Viral Strain	AAV-CMV-GFP-WPRE-pA	BrainVTA biotech	Custom-made	
Bacterial or Viral Strain	AAV-CMV-BAG3-GFP-WPRE-pA	BrainVTA biotech	Custom-Made	
Bacterial or Viral Strain	AAV-CAG-EGFP-U6-scramble-shRNA	ObiO biotech Shanghai	Custom-Made	
Bacterial or Viral Strain	AAV-CAG-EGFP-U6-shBAG3-1-3	ObiO biotech Shanghai	Custom-Made	
Organism/Strain	C57BL/6	Xiamen University Laboratory Animal Center	N/A	
Organism/Strain	5XFAD [B6SJL-Tg(APPsw ^{F1L} on, PSEN1 ^{M146L})1Mm]J	Model Animal Research Center of Nanjing University	N/A	
Organism/Strain	APP/PS1 [B6C3-Tg(APPsw, PSEN1 ^{dE9})85D]	Model Animal Research Center of Nanjing University	N/A	
Organism/Strain	Nestin-Cre [B6.Cg-Tg(Nes-cre)1Kln/J]	Model Animal Research Center of Nanjing University	N/A	
Organism/Strain	BAG3-conditional knockout (cKO) mice (BAC)	Beijing Biocytogen Co., Ltd	Custom-made	
Organism/Strain	C57BL/6	Animal and Plant Care Facility of the Hong Kong University of Science and Technology		
Organism/Strain	Camk2a ^{-/-} Ta [B6.CBA-Tg(Camk2a ^{-/-})1Mm]J	Jackson Laboratory	#003010	
Organism/Strain	APP/PS1 [B6C3-Tg(APPsw, PSEN1 ^{dE9})85D]	Jackson Laboratory	#34829-JAX	
Organism/Strain	p25 [C57BL/6-Tg(tetO-CDK5R1/GFP)337Lnt]	Jackson Laboratory	#005756	
Organism/Strain	CDK5-knockout [B6;129-Cdk5 ^{tm1} Kul/J]	Jackson Laboratory	#006388	
Biological Sample	Human autopsy tissues	NICHHD brain and Tissue Bank of Developmental Disorders at the University of Maryland, Baltimore, MD	Contract #N01-HD-4-3368 and N01-HD-4-3383	
Cell Line	HT-22 Mouse Hippocampal Neuronal Cell Line	Millipore	SCC129	
Cell Line	Neuro 2A	ATCC	ATCC® CCL-131™	
Cell Line	HEK293T	ATCC	ATCC® CRL-3216™	
Cell Line	HEK293FT	Thermo Fisher	R70007	
Chemical Compound or Drug	Roscovitine	Toocris	Cat. No. 1332	
Chemical Compound or Drug	Lipofectamine 2000	Thermo Fisher	11668027	
Chemical Compound or Drug	Lipofectamine LTX with Plus reagent	Thermo Fisher	15338100	
Commercial Assay Or Kit	RNeasy mini kit	Qiagen	74104	
Commercial Assay Or Kit	High-Capacity cDNA Reverse Transcription Kit	Applied Biosystems	4368814	
Commercial Assay Or Kit	SYBR Green PCR Master Mix	Applied Biosystems	4309155	
Commercial Assay Or Kit	FD Rapid Golgi Stain kit	FD NeuroTechnologies	PK401	
Commercial Assay Or Kit	Site-Directed Mutagenesis Kits (Quickchange)	Agilent Stratagene	200521	
Commercial Assay Or Kit	Lentivirus-Associated p24 ELISA Kit	Cell Biolabs	VPK-107	
Commercial Assay Or Kit	Micro BCA protein assay kit	Thermo Fisher	23235	
Commercial Assay Or Kit	Pierce™ GST Protein Interaction Pull-Down Kit	Thermo Fisher	21516	
Commercial Assay Or Kit	Titansphere Phos-TiO kit	Fisher Scientific	NC9738209	
Peptide, Recombinant Protein	Human amyloid-beta peptide (1-42)	Toocris	#1428	
Sequence-Based Reagent	Mouse Hspa1a siRNA	Thermo Fisher	AM16708	
Sequence-Based Reagent	Mouse Cdk5 siRNA	Thermo Fisher	AM16708	
Sequence-Based Reagent	Mouse Bag3 siRNA	Thermo Fisher	AM16708	
Software; Algorithm	Protein sequences alignment	Clustal Omega Platform	https://www.ebi.ac.uk/Tools/msa/clustalo/	
Software; Algorithm	Protein sequences identification	NCBI Gene database	https://www.ncbi.nlm.nih.gov/gene	
Software; Algorithm	Freeze Frame software	Actimetrics	N/A	
Software; Algorithm	Mini Analysis software	Synaptosoft, Inc	N/A	
Software; Algorithm	Graphpad Prism 5	Graphpad	N/A	
Transfected Construct	psPAX2	Addgene	#12260	
Transfected Construct	pMD2.G	Addgene	#12259	
Transfected Construct	GFP-BAG3-WT	Made in house	N/A	
Transfected Construct	GFP-BAG3-S297A	Made in house	N/A	
Transfected Construct	GFP-BAG3-S297D	Made in house	N/A	
Transfected Construct	GFP-BAG3-T285A	Made in house	N/A	
Transfected Construct	GST-BAG3-WT	Made in house	N/A	
Transfected Construct	GST-BAG3-S297A	Made in house	N/A	
Transfected Construct	GST-BAG3-297D	Made in house	N/A	
Other	Magnetic Dynabeads Protein G Immunoprecipitation Kit	Thermo Fisher	10007D	

Cyclin-Dependent Kinase 5-Dependent BAG3 Degradation Modulates Synaptic Protein Turnover

Supplement 1

Contents:

Detailed Supplemental Methods and Materials

Supplementary Figures

Supplementary Table Legends

Supplemental References

Journal Pre-proof

Detailed Supplemental Methods and Materials

Antibodies and chemical reagents

Antibodies against CDK5 (#2506), CDK substrate (#9477), PSD95 (#3450); cleaved caspase-3 (#9661); β -actin (#4970), GAPDH (#5174) and phospho-Rb (Ser807/811) (#9308) were purchased from Cell Signaling Technology. Anti-CDK5 (sc-6247); GFP (sc-8334); p35/p35 (sc-820/821); V5(sc-83849) and GAPDH (sc-47724) antibodies were purchased from Santa Cruz Biotechnology. Anti- α -tubulin (T5168); Synaptophysin (SAB4502906) and anti-Flag (M2) (A2220) antibodies were purchased from Sigma Aldrich. Anti-BAG3 (ab86298) and PSD95(ab12093), GLUR1(ab31232), GLUR2 (ab20673) and NR2B (ab65783) antibodies were purchased from Abcam. Anti-Syntaxin 1 (YT5440) antibody was purchased from Immunoway. Anti-Synapsin-I (AB1543), NR2A (#07-632), CDK5 (#05-364) antibodies were purchased from Millipore. Anti-GST (HRP-66001) antibody was purchased from ProteinTech. Anti-BAG1 (PA5-29585); BAG2 (PA5-30922); BAG3 (PA5-54239) and HSP70 (MA3-006) antibodies were purchased from ThermoFisher. Anti-beta-amyloid (GTX82974) and amyloid-precursor protein (GTX101336) antibodies were purchased from GeneTex.

The custom-made rabbit antibody against phosphorylated Ser297 of BAG3 was generated by ProSci Incorporated (Poway, CA). In brief, rabbits were inoculated with a BAG3 phospho-peptide (PLHSP(pS)PIRVH) to induce an immune response. Subsequent serum fractionation using both negative- and positive-affinity purification methods was performed to optimize the specificity for the targeted phospho-epitope.

Secondary antibodies used for immunocytochemistry assay were listed as follows: goat anti-mouse Alexa-488 and -594; as well as goat anti-rabbit Alexa-488 and -594 antibodies were purchased from ThermoFisher. Special reagents, such as human amyloid-beta peptide (1-42) (#1428) was purchased from Torcis. Magnetic Dynabeads for co-immunoprecipitation were purchased from ThermoFisher. Unless otherwise specified, all chemicals and reagents were purchased from Sigma.

Animal maintenance, brain tissue isolation, and primary neuron culture

Regarding to mouse colonies in Xiamen University: C57BL/6 mice were directly purchased from Xiamen University Laboratory Animal Center. The 5XFAD [B6SJL-Tg(APPswFLon, PSEN1*^{M146L}*^{L286V})6799Vas/Mmjax], APP/PS1 [B6C3-Tg(APP^{swe}, PSEN1^{dE9})85Dbo/Mmjax] AD-model, and Nestin-Cre [B6.Cg-Tg(Nes-cre)1Kln/J] were obtained from Model Animal Research Center of Nanjing University. BAG3-conditional knockout (cKO) mice (BAG3^{fl/fl}) were generated with custom service from Beijing Biocytogen Co., Ltd. All animal experiments were approved by and conducted in accordance with the guidelines of the Animal Ethics Committee of Xiamen University.

Mouse brain tissues were harvested as previously described (1). In brief, adult mice were anesthetized with intraperitoneal administration of 1.25% (vol/vol) Avertin at a dosage of 30 mL/kg body weight. The heart of each mouse was then surgically exposed; the left chamber

was catheterized; the right atrium was opened. Chilled physiological saline was perfused trans-cardially for 3 minutes to elute blood from the body. After perfusion, the cranial bones were opened; cortex and hippocampus tissues were harvested, snap-frozen in liquid nitrogen, and stored at -80 °C until use.

Primary neuronal culture was prepared as previously described (1). In brief, cortical neurons were disintegrated from cortical tissues of embryonic day 16.5 (E16.5) mouse pups (primary hippocampus neurons were disintegrated from hippocampal tissues of P0 mouse pups). Embryos were collected in ice-cold PBS-glucose, and the cortical or hippocampal lobes were excised. Meninges were removed and the tissues were placed in 1X trypsin solution for 10 minutes, with manual shaking at 5 min. After digestion, an equal volume of DMEM with 10% (vol/vol) FBS was added to inactivate the trypsin. Samples were then centrifuged at 2,500 rpm for 5 min. Supernatant was removed, followed by transferring the pellet to fresh Neurobasal medium supplemented with B-27, penicillin/streptomycin (1X) and L-glutamine (2mM; GlutaMAX, Invitrogen) prior to gentle re-suspension. Tissue was triturated 10 times through a 5-mL pipette and allowed to settle to the bottom of a 15-mL conical tube. Cells in solution above the pellet were removed. Surviving cells were identified by trypan blue exclusion and counted before plating on poly-L-lysine-coated (0.05 mg/mL) glass coverslips. Unless otherwise specified, cells were plated in 24-well plates at 50,000 cells per well and allowed to mature for over 7-10 days *in vitro* (DIV) before transfection or lentiviral transduction. For other experiments, cells were grown for a minimum of 14 days *in vitro* (DIV14) before drug-treatment experiments. Every 3-day half of the culture medium was replaced with an equal volume of fresh medium to sustain the culture.

Human brain tissues

Human autopsy tissues harvested from eight individuals diagnosed with AD and eight age-matched controls were obtained from the NICHD Brain and Tissue Bank of Developmental Disorders at the University of Maryland, Baltimore, MD [NICHD Brain Tissue Bank for Developmental Disorders and NICHD (Contract #N01-HD-4-3368 and N01-HD-4-3383)] (details on samples, are listed below). Frozen brain tissues were embedded in Tissue-Tek Cryo-O.C.T. compound and sectioned at 10 μ m. All AD cases were confirmed both clinically and by post-mortem examination. The average age of the subjects was 75 years for the AD patients and 72.5 years for non-demented controls (NDCs). The non-AD controls were free of any known CNS neurological diseases at the time of death.

Case Details

Sample ID	Disorder	Sex	Age (Years)	Race	Postmortem Interval (Hours)
4512	AD	M	77	Caucasian	3
1946	AD	M	68	Caucasian	5
5007	AD	F	76	Caucasian	15
5504	AD	F	73	Caucasian	22
4697	AD	M	78	Caucasian	23
4693	AD	F	70	Caucasian	12

5195	AD	M	80	Caucasian	9
5590	AD	F	78	Caucasian	17
4789	AD	F	72	Caucasian	19
5572	NDC	F	70	African American	24
5604	NDC	F	73	Caucasian	20
5661	NDC	M	70	African American	12
4921	NDC	F	73	Caucasian	13
5755	NDC	M	72	Caucasian	15
5830	NDC	M	75	Caucasian	18
5840	NDC	M	75	Caucasian	17

Sample preparation, LC-MS/MS and proteomics analyses

LC-MS/MS and proteomic analyses were performed as previously described with slight modifications (2, 3). Mouse primary cortical neurons pre-expressed with either GFP-only, GFP-tagged BAG3 or GFP-tagged HSP70 for 72 hours were harvested. Lysates were immunoprecipitated with anti-GFP antibody conjugated to magnetic Dynabeads® (Life Technologies). The enriched proteins were resolved by 7.5% SDS-PAGE gel. Lanes containing GFP-only or GFP-fused protein interacting proteins were cut into smaller fragments and washed with 25 mM NH₄HCO₃/ 50% Acetonitrile (ACN) until it became colorless. Gel fragments were shrunk in ACN for 15 minutes, centrifuged to remove supernatant. Proteins in the residual gel fragments were reduced in 10 mM DTT at 55°C for 45 minutes, followed by alkylation in 55 mM Iodoacetamide (IAA). Each segment was then digested with mass spectrometry grade Trypsin (Promega) in 1:50 (w/w) overnight at 37°C. Digested peptides were extracted using 25 mM NH₄HCO₃ and 5 % formic acid/ 60% ACN, speed dried and re-dissolved in 0.5% formic acid, which was then desalted in a μ C18 reverse-phase ZipTip (Millipore). Eluted samples were analyzed on a LTQ Velos mass spectrometer (Thermo Scientific), which coupled to a Thermo Accela LC with a nano-electrospray ionization source. One microgram of digested protein was enriched on a trap column (Zorbax X300 SB-C18, 5 x 0.3 mm, 5 μ m particle size) and separated on a C18 column (Thermo Bio-Basic-18, 150 x 0.1 mm, 300 Å pore size, 5 μ m particle size) at a flow rate of 220 μ L/min. The composition of LC solvent A was 0.1 % formic acid in water and solvent B was 0.1 % formic acid in acetonitrile. The LC mobile phase was maintained at 2% of solvent B for 2 minutes after sample loading. The gradient of the LC started by increasing solvent B from 2 % to 8 % for 8 minutes and then to 45 % for 33 minutes. After that, the gradient was quickly increased to 80 % within 2 minutes and then kept stabilized for 9 minutes; followed by a drop to 2 % within 1 minute and maintained as such for 9 minutes for equilibration before the next injection. For mass spectrometry analysis, each MS1 was followed by 5 MS2 of the 5 most intense ions observed in MS1 scan. The dynamic exclusion time was 60 seconds. Collision induced dissociation (CID) was used in MS2 and the normalized collision energy was set at 35%. Peptides and proteins were identified using the Mascot Server (Version 2.3, Matrix Science). Databases used was Swissprot/NCBI and the taxonomy was set as mouse. The search criteria were set as follows: (1) trypsin digestion with two allowed missed cleavage; carbamidomethylation on cysteine as a fixed modification, and oxidation on methionine as variable modification.

SILAC phospho-proteomic analysis

Global phosphoproteomic analysis was performed as described previously with slight modifications (4, 5). SILAC N2a cells were grown for 6 doublings in either one of the SILAC media. Control cultures were grown in medium containing unlabeled amino acids (R0K0). Experimental cultures were grown in heavy weighted amino acids (arginine with six ^{13}C plus four ^{15}N substitutions and lysine with four ^2H and two ^{15}N substitutions – R10K8). In all cultures, 98% labeling efficiency was achieved. Cells grown in the R10K8 medium were transfected to overexpress with p35 alone or both CDK5 and p35. Cultures were maintained for an additional 48 hours before harvesting. 1.5 mg of cell lysates from both cultures were mixed in a 1:1 ratio and separated by NuPAGE 10% Bis-Tris Gel electrophoresis (Thermo Fisher). Gels were sliced into 10 pieces, followed by reduction with DTT, alkylation with iodoacetamide and digestion with trypsin (Promega) overnight at 37°C. Peptides were extracted twice with 5% formic acid, 60% acetonitrile (CAN) and dried under vacuum. Extracted peptides were then subjected to phosphoproteins enrichment, using Titansphere Phos-TiO kit (Fisher Scientific) following manufacturer's instructions. Enriched phosphopeptides were then analyzed by NanoLC-MS/MS (Ultimate 3000 RLSCnano System linked to Velos LTQ Orbitrap, Thermo Fisher). In brief, peptides were solubilized in 0.1% Trifluoroacetic acid (TFA) and loaded on to a self-made fused silica trap-column of 100umX2cm packed with Magic C18 AQ (5um bead size, 200Å pore size, Michrom Bioresources, Inc.) and washed with 0.2% formic acid at a flow-rate of 10ul/min for 5 min. Retained peptides were separated on a fused silica column of 75um x 50cm self-packed with Magic C18 AQ (3um bead size, 200Å pore size, Michrom Bioresources, Inc.) using a linear gradient from 4 to 50% B (A: 0.1% formic acid, B: 0.08% formic acid, 80% ACN) in 155 min at a flow-rate of 300 nl/min. A top 10 method was used for mass spectrometry. For each cycle, one full MS was scanned in the Orbitrap with a resolution of 60000 from 300-2000 m/z followed by HCD fragmentation of 10 most intense peaks with collision energy of 40% and scanned in Orbitrap with 7500 resolutions. Data-dependent acquisition was set for repeated count of 2 and exclusion of 60 sec. MS/MS spectra were searched via MASCOT 2.3 against IPI mouse database v. 3.26 using the following parameters: precursor mass tolerance 10 ppm, fragment mass tolerance: 0.01 Dalton, static modification of carbamidomethylation on cysteine (+57.0214) and dynamic modification for phosphorylation on serine, threonine and tyrosine (+79.96630), methionine oxidation (+15.9949), $^{13}\text{C}_6$ -arginine (+6.02), $^{13}\text{C}_6^{15}\text{N}_4$ -arginine (+10.008), $^2\text{H}_4$ -lysine (+4.025) and $^{13}\text{C}_6^{15}\text{N}_2$ -lysine (+8.014). The peptide identification results were filtered using FDR of 1% and only the top match was used for each identified spectrum. Precursor quantitation was performed using Proteome discoverer 1.2 with mass precision 3ppm.

Intracranial injections into neonatal mice

Procedures were performed as previously described with slight modification (6). Within 6 hours of birth, neonates were collected from cages, and anesthetized in aluminum foil immersed in ice for 3-5 min before injection. Cryo-anesthesia was confirmed when pup movements were ceased, and their skin color changed from pink to light purple. Injection of AAV virus-carrying (1) scrambled shRNA and BAG3-targeting shRNA shuttles; or (2) GFP-vector or GFP-tagged BAG3 shuttles, in viral titers around 7.35×10^{12} was done to two

lateral ventricles. After injection, pups were monitored and allowed to completely recover on a warming blanket prior to returning to their home cage. At 30-day post-injection, mice were sacrificed, and brains were harvested for Golgi staining and electrophysiology experiments. Alternatively, some mice were kept until 60-days post-injection and subjected to behavioral tests (which almost lasted for an additional month) prior to being sacrificed for additional biochemical analyses around Day90 post-injection.

Western blotting and co-immunoprecipitation

Immunoblotting and co-immunoprecipitation were performed as described previously (1). Briefly, harvested cells were homogenized in ice-cold NP-40 lysis buffer with protease inhibitor mix (Roche). The samples were centrifuged at 12000g for 15 min at 4°C. The supernatant was collected, and total protein levels were quantified by micro BCA protein assay kit (Thermo Fisher). For Western blots, the lysates were separated with SDS-PAGE followed by transferring onto nitrocellulose membranes. Membranes were blocked with 5% non-fat milk in TBST and then probed with primary antibodies at different concentrations according to manufacturer's instructions overnight at 4°C. On the next day, membranes were washed thrice with TBST, followed by incubation with horseradish peroxidase-linked secondary antibodies for 1 hour at room temperature. After another round of washing with TBST, chemiluminescent Western ECL detection reagents (Pierce) was used to illuminate the signals. Intensities of immune-reactive bands were quantified using the Image J software (NIH). For immunoprecipitation, cell lysates were incubated with immunoprecipitation antibody at 4°C for 4 hours, followed by overnight incubation with protein G beads. The beads were then washed five times with ice-cold NP-40 lysis buffer, and the bound proteins were analyzed by SDS-PAGE and immunoblot analysis as mentioned above.

Immunohistochemistry and immunocytochemistry

Procedures were performed as previously described with slight modifications (1, 7). For immunostaining, primary neurons were grown on 13-mm coverslips (Marienfeld) in 24-well plates. At appropriate times cultures were fixed with fresh 4% (wt/vol) paraformaldehyde (Sigma-Aldrich) for 10 min, followed by permeabilization with 0.3% Triton X-100 in PBS for 10 min. After blocking with 5% (wt/vol) BSA in PBS for 1 hour, primary antibodies were added and allowed incubation overnight at 4 °C. The following day, coverslips were washed three times (10 minutes each) with PBS. After rinsing, secondary antibodies were added and incubated for 1 hour at room temperature. Three additional washes with PBS were done to remove excess secondary antibodies. The coverslips were then inverted and mounted on glass slides using the ProLong Gold Antifade Reagent (Thermo Fisher). Immunofluorescence was analyzed and Z-stacked maximum projected images were photographed using a TCS Sp8 confocal microscope (Leica Microsystems Inc.).

For immunostaining of brain sections, antigen retrieval was performed by treating the mounted cryostat sections with citrate buffer at 95 °C for 15 minutes followed by cooling to room temperature for 1 hour. Sections were rinsed in PBS, blocked with 5% (vol/vol) donkey serum/PBS for 1 hour before immune-staining procedure as above.

GST-pull down

Glutathione-S-transferase (GST) fusion protein expression pull-down served as an affinity capture of one or more proteins (either defined or unknown) in solution by its interaction with the GST fusion probe protein and subsequent collection of the interacting proteins through the binding of GST to glutathione-coupled beads. The protocol was performed according to the manufacturer's instructions (ThermoFisher).

***In vitro* and intracellular CDK5 kinase assay**

For *in vitro* CDK5 kinase assays were carried out as described in the New England Biolabs protocol. Briefly, recombinant active CDK5/P35 complex was incubated in the following reaction conditions: 60 mM HEPES-NaOH, pH 7.5, 3 mM MgCl₂, 3 mM MnCl₂, 3 M sodium vanadate, 1.2 mM DTT, ATP, 1 µg of full-length GST-BAG3, GST-BAG3-S297A, or GST-BAG3-T285A were added as the substrate. Kinase reactions were separated by SDS-PAGE gel electrophoresis and analyzed by autoradiography or by immunoblotting using the CDK substrates antibody. For CDK5 activity measurement inside cells treated under different conditions, active CDK5 immunoprecipitation and kinase assay were performed as previously described (8).

Preparation of synaptosomal and PSD fractions

Synaptosomal and PSD fractions were prepared as previously described (9). Briefly, primary cortical neurons (DIV14) were collected in cold HEPES-buffered sucrose (HBS=0.32M sucrose and 25mM 4-(2-hydroxyethyl)-1-piperazineethanesulfonic acid (HEPES), pH=7.4). The homogenates were centrifuged at 500g for 5 min to separate the supernatant (S1) from the nuclei and large debris fraction. The S1 fraction was centrifuged at 10,000g for 12min to separate the supernatant (S2, light membrane and cytosolic fraction) and the pellet (P2, crude synaptosomal fraction). The P2 fraction was re-suspended in cold HBS buffer (25 mM HEPES, pH=7.4, and 150mM NaCl) to obtain the synaptosomal fraction. The PSD fraction was prepared by solubilizing the synaptosomal fraction in 1% Triton HBS buffer and centrifuging at 10,000g for 20 min. Solubilized pellets were re-dissolved in 3% SDS-containing HBS buffer and used for subsequent analyses.

Cell culture and transfection

Cell culture and transfection were performed as previously described (1, 7). Mouse neuroblastoma N2A, hippocampal cell line HT22 and Human HEK293T cells were cultured in high glucose DMEM medium containing 10% FBS, 100 unit/ml penicillin, and 100unit/ml streptomycin. Cells were maintained at 37°C and 5% CO₂. Primary cortical neurons were cultured as mentioned above. For transfection into cell lines, DNA constructs were transfected with Lipofectamine 2000 (Thermo Fisher) following the manufacturer's protocol. For transfection into primary neuronal cultures, DNA constructs were transfected with Lipofectamine LTX (Thermo Fisher) in the presence of Plus Reagent following the manufacturer's protocol. At 5 hours after transfection, cells were refreshed with a new culture medium (or conditioned medium for primary neurons) and further incubated for 48-72 hours to allow recovery and ectopic expression of transfected constructs.

Quantitative RT-PCR (qPCR) analysis

Quantitative RT-PCR analysis was performed as previously described with slight modifications (1). Total cellular RNA was isolated from brain cortex tissues or cultured cells using the RNeasy mini kit (Qiagen) following the manufacturer's protocol. RNA was then reverse-transcribed using the High-Capacity cDNA Reverse Transcription Kit (Applied Biosystems) according to the manufacturer's instructions. The resulting cDNA was analyzed by qRT-PCR using SYBR Green PCR Master Mix (Applied Biosystems). All reactions were performed in a Roche LightCycler (LC) 480 instrument using the following protocol: pre-incubation at 95 °C for 15 min (1 cycle); denaturation at 94 °C for 15 seconds, annealing and extension at 55 °C for 30 seconds (40 cycles), melting at 95 °C for 5 seconds, 65 °C for 60 seconds and 95 °C continues (1 cycle) followed by cooling at 40 °C for 30 seconds. The specificity of the primers was confirmed by observing a single melting point peak. qPCR efficiency was calculated from the slope was between 95 and 105% with co-efficiency of reaction $R^2=0.98-0.99$. A total of 7-9 biological replicates x 4 technical replicates were performed for each treatment group. Data were analyzed using the comparative Ct method ($\Delta\Delta C_t$ method).

Golgi staining and Dendritic and spine analyses

Golgi staining was performed using the FD Rapid Golgi Stain kit (FD Neuro Technologies). The experiments were performed in accordance with the protocol of the Kit. In brief, freshly dissected brains were immersed in solution A and B in FD Rapid Golgi Stain kit for 2 weeks at room temperature (A switch from solution A to B occurred on Day 1). After that, samples were transferred to solution C for incubation at 4°C for 24 hours. After 24 hours, samples were refreshed in new solution C to allow an extra round of incubation for 3-5 days at 4 °C. Brains were sliced with a thickness of 150 μm . The Golgi-stained neurons and dendritic segments in hippocampal CA1 and layer II/III of the cortex were imaged with the Axio Imager microscope (Carl Zeiss). The Extended Focus module was used to compress Z-stack images into one single image. The pyramidal neurons in cortical layers II/III and in the CA1 region of the hippocampus were also analyzed. Neurons were randomly selected per region in each mouse. Two segments were randomly chosen per neuron from both the apical oblique and basal shaft (BS) dendrites, and the numbers of spines were counted and quantified in blind.

Plasmids, small interference RNA (siRNA) and BAG3-AAV

Site-directed mutagenesis (Stratagene) was used to generate pointed-mutated BAG3 constructs, including GFP-BAG3-S297A, GFP-BAG3-S297D and GFP-BAG3-T285A. For the generation of GST-tagged BAG3 constructs, including GST-BAG3-WT, GST-BAG3-S297A and GST-BAG-297D, wild type or point-mutated BAG3 fragments were generated by the PCR method, followed by sub-cloning into the Mrfp-GST-4T-1 and a lentiviral pLX304 V5-fusion backbone expression vector. For the GFP backbone, FLAG/GFP-p25, FLAG/GFP-p35, FLAG/GFP-CDK5 vectors were obtained or generated as previously described (10, 11). The EGFP-HSP70 (HSPA1A) (#15215) was obtained from Addgene (12). Gene-specific siRNAs targeting *Hspa1a*, *Cdk5* and *Bag3* were purchased from Thermo Fisher. The AAV-based shRNA against BAG3, including

AAV-CAG-EGFP-U6-scramble-shRNA and AAV-CAG-EGFP-U6-shBAG3-1-3 were purchased from OBiO biotech Shanghai. The AAV-based construct for overexpression of BAG3, including the AAV-CMV-GFP-WPRE-pA (backbone) and AAV-CMV-BAG3-GFP-WPRE-pA were purchased from BrainVTA biotech (Wuhan, China).

Production and purification of AAV virus

AAV virus were produced and purified as previously described with slight modifications (13). The pAAVs and two helper plasmids were used for AAV production: 1. pHelper (Stratagene) expresses the adenovirus helper functions (E2A, E4 and VA genes), and the other helper plasmid, 2. pBSIISK-R2C1, expressing the replication protein of AAV serotype 2 (Rep2) and the capsid protein of AAV serotype 1 (Cap1), was newly prepared by inserting the following fusion sequences into the XhoI/NotI sites of pBSIISK: 1) nucleotides 146–2,202 of wild-type AAV2 genome (GenBank accession number, AF043303.1); 2) nucleotides 2,223–4,433 of AAV1 (AF063497.1); and 3) nucleotides 4,438–4,534 of AAV2. Production and purification of AAV were performed as reported previously. Briefly, pAAVs, pHelper, and pBSIISK-R2C1 were co-transfected into HEK293T cells (RCB2202, Riken, Japan) by using polyethyleneimine (23966; Polysciences, Inc., Warrington, PA). The medium was replaced 6 h after transfection with Dulbecco's modified Eagle's medium (11965–092; Life Technologies) containing 10% fetal bovine serum, 4 mM l-glutamine (25030–081; Life Technologies), 2 mM GlutaMAX™ (35050–061; Life Technologies), 0.1 M non-essential amino acids (35050–061; Life Technologies), and 1 mM sodium pyruvate (11360–070; Life Technologies). Cells containing virus particles were collected 72 h after medium replacement. After extraction by three cycles of freeze-and-thaw, the virus particles were purified from a crude lysate of the cells by ultracentrifugation with OptiPrep (AXS-1114542; Axis-Shield, Oslo, Norway) and then concentrated by ultrafiltration with Amicon Ultra-15 Centrifugal Filter Unit with Ultracel-50 membrane (UFC905024; Merck Millipore, Darmstadt, Germany).

Lentivirus production and transduction

Lentivirus stocks were produced as previously described with slight modifications (14). Human embryonic kidney 293FT cells (Invitrogen) were transfected using Lipofectamine 2000 (Thermo Fisher) with the expression of two helper plasmids: psPAX2 and pMD2.G. Ten micrograms of the transfer vector, 5 µg pMD2.G and 5 µg psPAX2 of DNA were used per 10-cm plate. Forty-eight hours after transfection, the supernatants of four plates were pooled, centrifuged at 780 x g for 5 minutes, filtered through a 0.45-µm pore size filter, and further centrifuged at 24,000 rpm for 2 hours. The resulting pellet was re-suspended in 100 µL of PBS. Lentivirus titration was performed with a p24 ELISA (Cell BioLabs). Lentivirus transduction to primary cortical neurons was performed on DIV5-6 at titer range 10^7 IU/ml. In most experiments, cultures were infected overnight, rinsed twice with virus-free medium the next morning and incubated in normal culturing medium for another 48-72 hour prior assay.

Multiple protein sequence alignment

Protein sequences of BAG3 in *Homo sapiens* (human) [NP_000427.2], *Pan troglodytes* (chimpanzee) [XP_508072.3], *Mus musculus* (mouse) [NP_038891.4] *Macaca mulatta* (Rhesus monkey) [NP_001252986.1] and *Rattus norvegicus* (rat) [NP_001011936.1] were

obtained from the NCBI-Gene database <https://www.ncbi.nlm.nih.gov/gene>. Multiple protein sequence alignment was performed on the Clustal Omega platform <https://www.ebi.ac.uk/Tools/msa/clustalo/> (15). Conserved S/TP sites among all the species analyzed were manually identified for subsequent analysis.

Electrophysiological recording

Brain slices were prepared as previously reported with slight modifications (Wen *et al.*, 2011). In brief, transverse hippocampal slices (0.40 mm) were prepared using a Vibroslice (VT 1000S; Leica) in an ice-cold solution containing 64 mM NaCl, 2.5 mM KCl, 1.25 mM NaH₂PO₄, 10 mM MgSO₄, 0.5 mM CaCl₂, 26 mM NaHCO₃, 10 mM glucose, and 120 mM sucrose. Slices were allowed to recover for 30 min at 32°C and then at room temperature (25 ± 1°C) for at least 1-hour prior initiation of recording in the artificial cerebrospinal fluid (aCSF) containing 126 mM NaCl, 2.5 mM KCl, 1.25 mM NaH₂PO₄, 2 mM MgSO₄, 2 mM CaCl₂, 26 mM NaHCO₃, and 10 mM glucose. Slices were transferred to the recording chamber and perfused with aCSF (2 ml/min) at 32°C. All solutions were saturated with 95% O₂/5% CO₂ (volume/volume). fEPSPs were evoked in the CA1 stratum radiatum by stimulating the SCs pathway with a two-concentric bipolar stimulating electrode (25-mm pole separation; FHC, Inc) and were recorded using a MultiClamp 700B amplifier (Molecular Devices) with aCSF-filled glass pipettes. Test stimuli consisted of monophasic 100-μs pulses of constant currents (with intensity adjusted to produce 25% of the maximum response) at a frequency of 0.0167 Hz were used. The strength of synaptic transmission was determined by measuring the initial (10–60% rising phase) slope of fEPSPs. LTP in the CA1 area was induced by one train of 100-Hz stimuli with the same intensity of the test stimulus, and a cut was made between CA1 and CA3 in hippocampal slices to prevent the propagation of epileptiform activity.

Whole-cell patch-clamp recordings were performed on CA1 pyramidal neurons which were visualized using an infrared differential interference contrast microscope with a 40× water immersion lens and an infrared-sensitive charge-coupled device camera. All experiments were conducted in neurons located within the cell-dense band CA1 region. Whole-cell patch-clamp recordings were performed using an amplifier (Axon Multiclamp 700B) and digitized by pClamp software (version 10.5; Molecular Devices). Both mEPSCs and mIPSCs were recorded at a holding potential of -65 mV. For mEPSC recording, glass pipettes were filled with the solution containing 120 mM K-gluconate, 20 mM KCl, 10 mM Hepes, 0.1 mM EGTA, 2 mM MgCl₂, 10 mM sodium phosphocreatine, 0.2 mM leupeptin, 4 mM Mg-ATP, and 0.3 mM Na-GTP, pH 7.3 (280 mOsm). For mIPSC recording, the same pipette solution was used except that the K-gluconate was substituted with 140 mM KCl (final concentration). NMDA receptor-mediated mEPSCs were recorded in a modified aCSF (0 mM MgSO₄, 5 mM KCl, and 1.6 mM CaCl₂). For evoked EPSC (eEPSC) and eIPSC recording, K-gluconate was substituted with 120 mM CsCH₃SO₃, and 5 mM lidocaine N-ethylchloride (QX-314) was added in the pipette. AMPA and NMDA receptor-mediated EPSCs were recorded at a holding potential of -65 mV and +40 mV, respectively; eIPSCs were recorded at a holding potential of -65 mV. 1 μM tetrodotoxin was included in the perfusion solution for mEPSC and mIPSC recording. For mEPSC and eEPSC recordings, 20 μM bicuculline was used to block GABA_A

receptor-mediated currents, and NMDA receptor-mediated eEPSCs were recorded in the presence of 20 μM 6-cyano-7-nitroquinoxaline-2,3-dione (CNQX). For mIPSC and eIPSC recording, 50 μM DL-2-amino-5-phosphonovaleric acid and 20 μM CNQX were supplemented to block NMDA and AMPA receptors, respectively. Stock solutions of all drugs were diluted to working concentrations in the extracellular solution immediately before use and applied by continuous superfusion. eEPSCs and eIPSCs were generated with a two-concentric bipolar stimulating electrode (FHC, Inc) positioned 200-300 μm from the neuron under-recording. Data were filtered at 2 kHz and sampled at 10 kHz. Neurons with a resting potential of at least -60 mV and resistance fluctuated within 15% of initial values (<20 M Ω) were analyzed. Mini events were analyzed with MiniAnalysis software (Synaptosoft, Inc.).

Animal behavioral tests

All tests were performed as previously described with slight modifications (16). At 60 days after injection with AAV virus, mice were subjected to various behavioral tests. All mice were housed in groups of five per cage. All behavioral tests were performed during the light phase of the circadian cycle between 09:00 and 17:00. All behavioral testing began on Day 8 of the course and mice were allowed 2 hours to habituate to the testing rooms before tests. Experiments were performed blind to the genotype when behavioral tests were carried out. With an overhead camera and the Freeze Frame software (Actimetrics), learning and memory performance were assessed using the Morris water maze, T/Y maze; novel object recognition tests; fear conditioning and freezing behavior were measured as well. Followed by these, experimental mice were also subjected to open field test, elevated plus maze test, forced swim test and rotarod test.

Morris water maze test. The Morris water maze test was conducted as described previously (17). Briefly, a blue circular tank (90 cm (diameter)*35 cm (high)) was filled with water (~22°C), and a platform (10 cm in diameter) was submerged 1 cm beneath the surface of the water in a target quadrant. The walls surrounding the tank contained bright and contrasting shapes that served as reference cues. Training was conducted over 7 consecutive days with four trials/day using an inter-trial interval of 1–1.5 min. Mice were placed randomly into each of four starting locations for each of four daily training trials. In each trial, mice swam until they found the hidden platform or were gently guided to it by the experimenter if not found within 60 seconds. Mice remained on the platform for 15 seconds before returning to the home cage. Daily data were averaged across the four trials. On day 7, a probe trial was conducted and the hidden platform was removed, mice were placed in the pool and allowed to swim for 60 seconds. The time spent in each of the four quadrants, and the number of target (platform) area crossings, were recorded.

T/Y maze. The T/Y-maze was used for the evaluation of spontaneous alternation for spatial working memory in mice. Each session began with the placement of the mouse at the center of the maze. The mouse was allowed to explore the three arms for 5 min freely. Arm entry was defined as all four limbs within the arm. A triad was defined as a set of three arm entries when each entry was to a different arm of the maze. Total travel distance, the number of arm

entries and the number of triads were recorded. Spontaneous alternations were defined as consecutive triplets of different arm choices.

Novel object recognition test. The novel object recognition test is based on the innate tendency of rodents to explore novel objects over familiar ones differentially. The test was performed as previously described (18). On the first day, mice were placed into a Plexiglas rectangular cage (40cm (L) × 40cm (W) × 40cm (H)) for 10 min. On the second day, mice were presented with two of the same objects, indicated as A and B. Twenty-four hours later, the mice were exposed to two different objects: A and C, with C indicating a novel object. All objects were rinsed with ethanol and allowed to dry between trials and before the first trial. All testing and training sessions were videotaped and analyzed in blind to the treatment group of the animals. Object exploration was defined as each instance in which a mouse's nose touched the object or was oriented toward and within 2 cm of the object. Exploratory activity within the experimental arena was measured over a five- minute trial with a computer timer.

Open-field test. Mice were placed in the center of an open-field arena (40cm (L) × 40cm (W) × 40cm (H)) for 10 min. During the experiments, the entire open field was video recorded. Total travel distance and time spent in the center areas of the maze were computed by a Smart 3.0 video tracking system (Panlab, Harvard Apparatus).

Elevated plus maze test. Mice were placed at the center of a white Plexiglas elevated plus maze (30 cm (Long) × 6 cm (Wide) × 15cm (High)) and were allowed to explore for 5 minutes (19). The Mice were monitored using CleverSys TopScan Software, and time spent in and number of entries into the open and closed arms were measured.

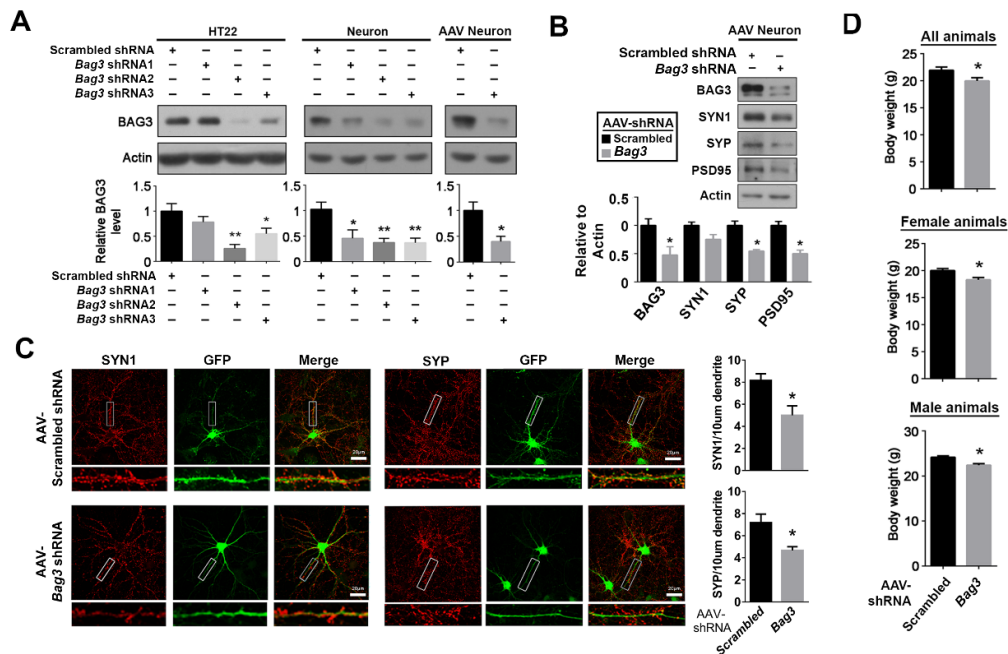
Rotarod test. Mice were placed on a stationary rotarod (IITC Life Sciences) in a well-lit room that was then activated and accelerated from 0 to 45 revolutions/ min over 5 min. The latency of mice to fall off the rod or taking one revolution was measured. Trials were repeated four times with intertribal intervals of 30 minutes over a single day.

Forced swim test. The forced swim test was used for evaluation of the depressive-like behaviors. The tanks (15cm (D) × 30cm (H)) were filled with tap water set at 22°C. Mice were placed in the water and their escape-related mobility behavior was measured for 8 min.

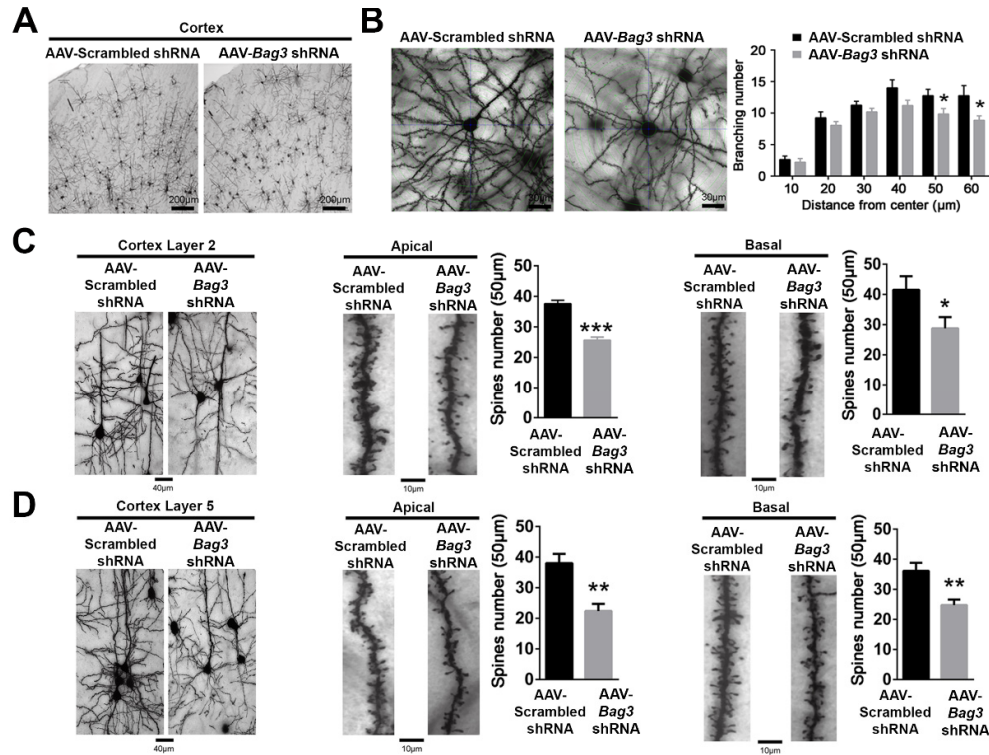
Quantitation and statistical analysis

All data were obtained from at least three different preparations. Each preparation contains a biological sample number not less than 3. Statistical analysis of the data was performed with an unpaired Student's t-test or a one-way ANOVA using Graphpad Prism 5. Data are presented as the Mean ± SEM. P values <0.05 represents statistical significance.

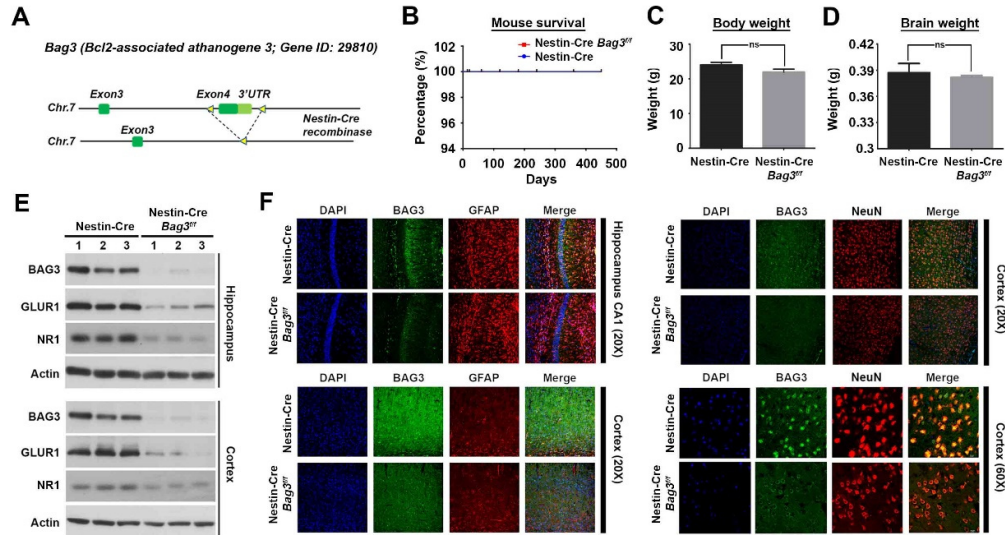
Supplementary Figures



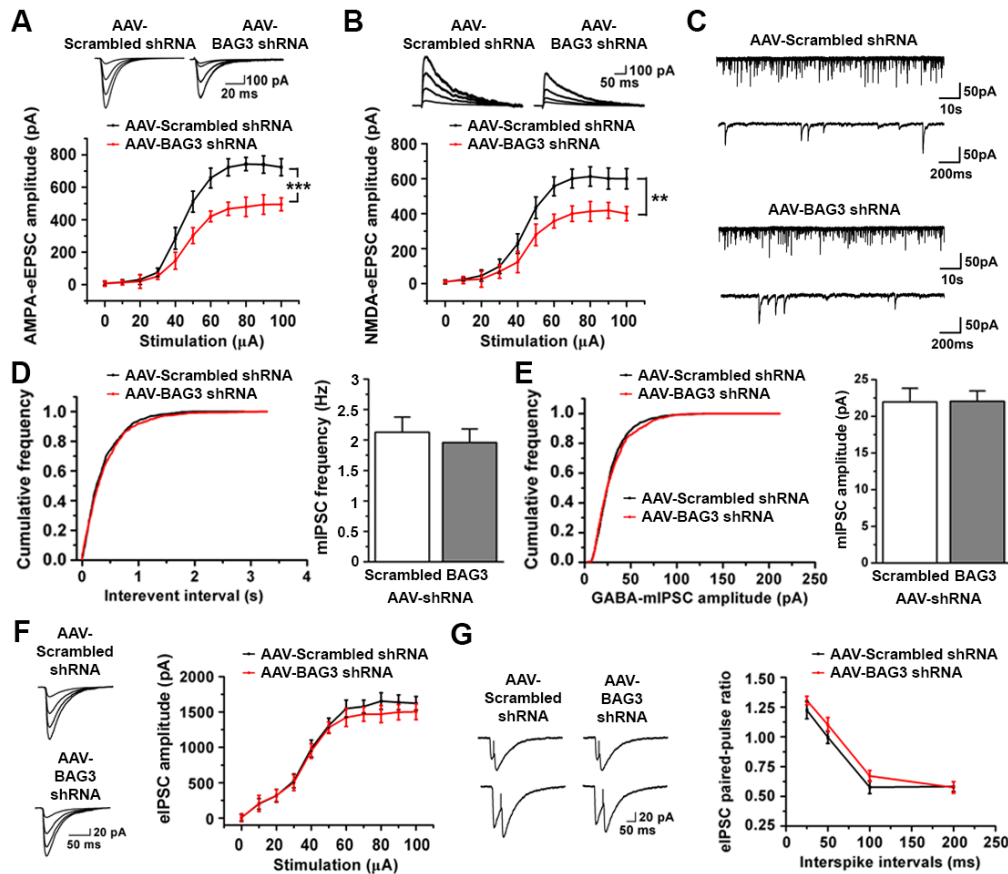
Supplementary Figure S1. *Bag3* knockdown reduced synapses in neurons. (A) Representative blots showing the efficiency of *Bag3* knockdown in HT22 cells or primary neurons transfected with the shRNA shuttles, and that by AAV-transduction to primary neurons. Quantification is shown (N=6). (B) Representative blots showing changes in levels of SYN1, SYP and PSD95 in primary neurons upon *Bag3* knockdown. Quantification is shown (N=6). (C) Representative immunocytochemical images of neurons showing changes in SYN1 and SYP signal abundance on neurites upon *Bag3* knockdown. Quantification is shown (N=6). (D) Bodyweight assessment in mice on Day 30 after receiving AAV injection to the prefrontal cortex and hippocampal area (N=6). Unless otherwise specified, all experiments were performed with at least 3 biological repeats; each individual assay was performed three times at least. * $P < 0.05$, ** $P < 0.01$, *** $P < 0.001$, ns=non-significant. Data represent the mean \pm SEM.



Supplementary Figure S2. Golgi staining analysis in structure and morphology of prefrontal cortex and primary neurons. Golgi staining analysis of effects of *Bag3* knockdown on neuronal morphology in (A) the brain prefrontal cortex region and (B) cultured primary cortical neurons. Quantification of neurite branching numbers relative to the distance from center is shown (N=6). (C-D) Representative images showing the changes in the complexity of neurite structures and the number of dendritic spines in cortical neurons located in (C) layer 2 and (D) layer 5 of the prefrontal cortex region. Quantification of spines number is shown (N=6). Unless otherwise specified, all experiments were performed with at least 3 biological repeats; each individual assay was performed three times at least. * $P < 0.05$, ** $P < 0.01$, *** $P < 0.001$, ns=non-significant. Data represent the mean \pm SEM.



Supplementary Figure S3. *Bag3* conditional knockout mice showed reduced synaptic abundance, cognitive and memory deficits. (A) Schematic diagram showing the design which selective knockout of *Bag3* in neural lineage was achieved by mating *Bag3^{fl/fl}* mice with Nestin-Cre mice. Exon 4 of *Bag3* was excised by Cre-recombinase. (B) Survival curves; (C) body and brain weights of Nestin-Cre controls and Nestin-Cre *Bag3^{fl/fl}* mice (N=6). (E) Representative blots showing changes of GLUR1 and NR1 levels in response to *Bag3* conditional knockout in cortex and hippocampal tissues (N=6). (F) Representative immunohistochemistry images showing the cellular location and levels of BAG3 in both hippocampal and cortex regions of brain samples harvested from Nestin-Cre controls and Nestin-Cre *Bag3^{fl/fl}* mice (N=8-16). Unless otherwise specified, all experiments were performed with at least 3 biological repeats; each individual assay was performed three times at least. * $P < 0.05$, ** $P < 0.01$, *** $P < 0.001$, ns=non-significant. Data represent the mean \pm SEM.

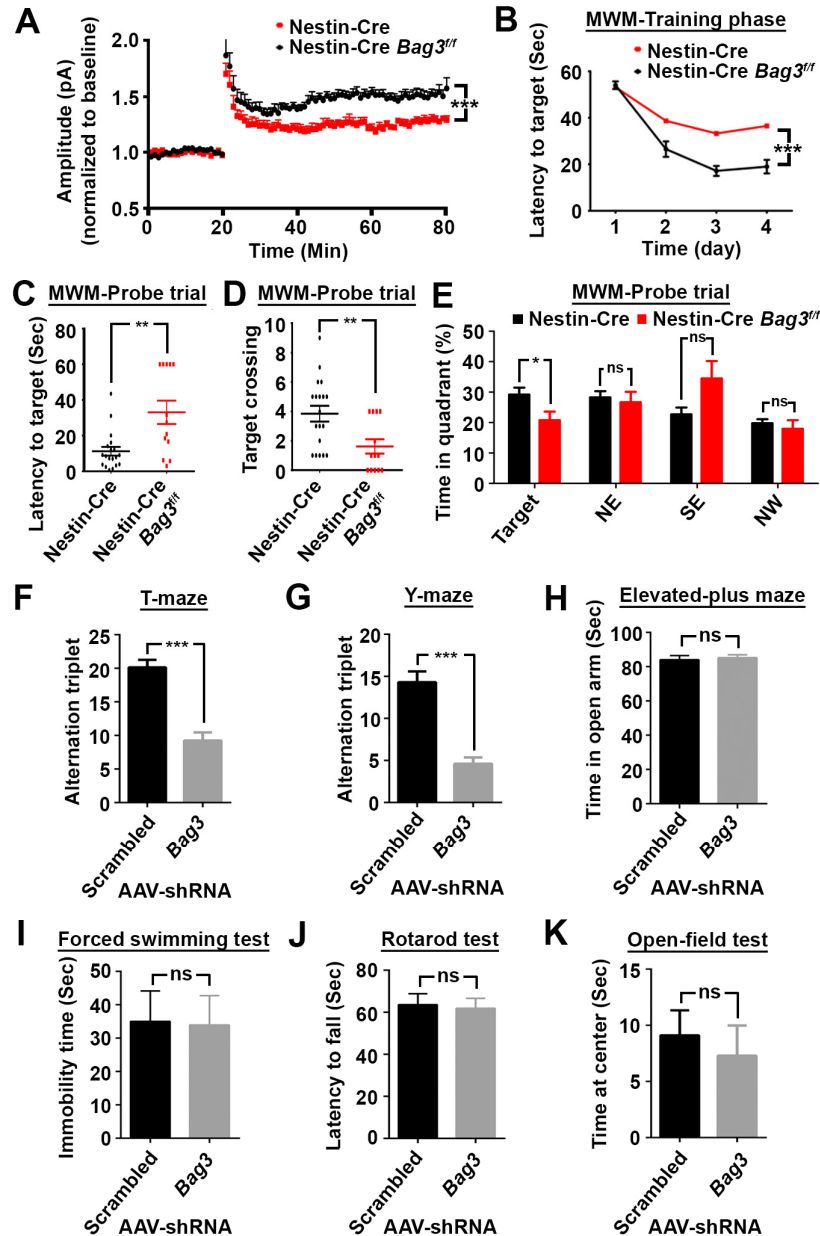


Supplementary Figure S4. BAG3 is crucial for mediating excitatory but not inhibitory neurotransmissions.

Electrophysiology recordings were performed on brain slices harvested from mice which had stereotaxically injected AAV carrying either scramble or *Bag3* shRNA shuttle. All experiments were performed on Day30 post-injection. (A) Representative traces of AMPA receptor-mediated eEPSC and quantitative analysis of eEPSC amplitude in response to increases in stimulation intensity are shown. (B) Representative traces of NMDA receptor-mediated eEPSC and quantitative analysis of eEPSC amplitude in response to increases in stimulation intensity are shown. AMPA and NMDA receptor-mediated EPSCs were recorded at a holding potential of -65 mV and +40 mV, respectively. The stimulation intensities for each trace were 20, 40, 50 and 80 μA (saturating stimulus) (N=8-12). (C) Representative traces of mIPSCs in mice stereotaxically injected AAV carrying either scrambled or *Bag3* shRNA. (D) Cumulative frequency plots of the inter-event interval (left) and quantitative analysis of the mean mIPSCs frequency (right). (E) Cumulative distribution plots (left) and mean mIPSC amplitude (right). (F) Representative traces of eIPSCs (20, 40, 50, and 80 μA) and quantification analysis of the eIPSC amplitude in response to increases in stimulation intensity are shown. (G) Representative traces (left) and quantification analysis of eIPSC paired-pulse ratio (right). The inter-spike intervals were 25, 50, 100 and 200 ms and signals were recorded from the whole-cell recordings of the hippocampal CA1 pyramidal neurons. Data were analyzed by unpaired t-test (for mean mIPSC amplitude and frequency), Kolmogorov–Smirnov test (for mIPSC cumulative histograms), and repeated measures (for eIPSC amplitude and paired-pulse ratio). Unless otherwise specified, all experiments were

performed with at least 3 biological repeats; each individual assay was performed three times at least. * $P < 0.05$, ** $P < 0.01$, *** $P < 0.001$, ns=non-significant. Data represent the mean \pm SEM, N=8-13.

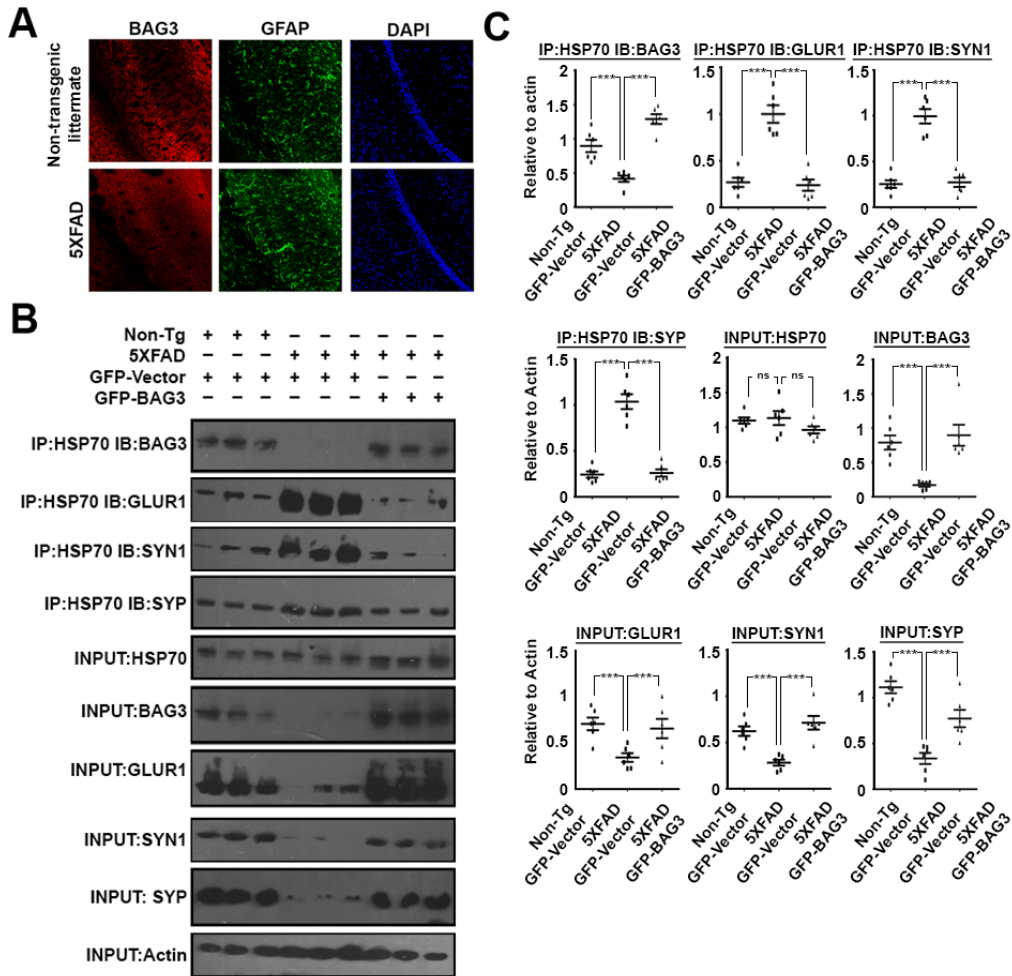
Journal Pre-proof



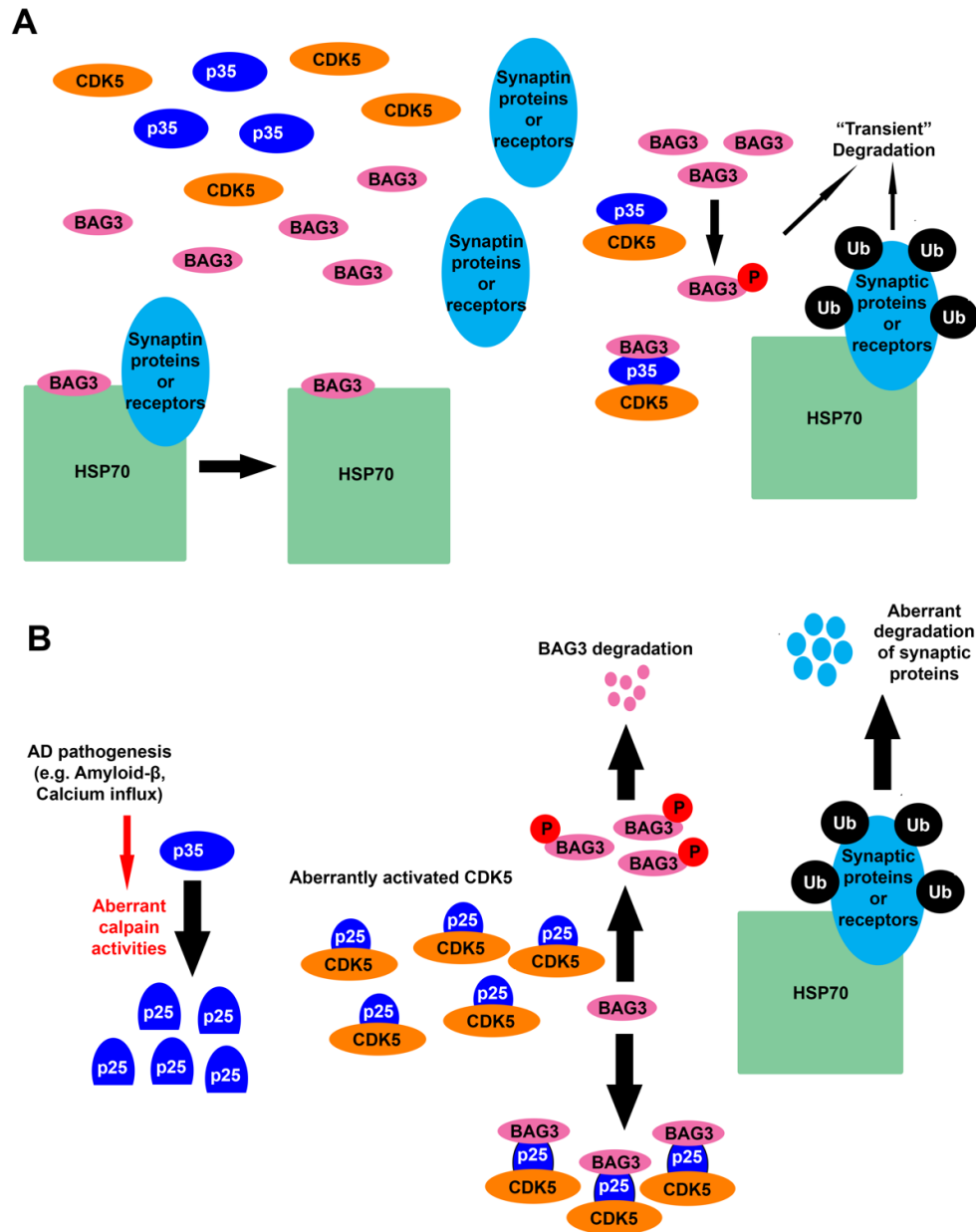
Supplementary Figure S5. BAG3 is crucial for memory and cognitive function. (A) LTP was measured in Nestin-Cre control or Nestin-Cre *Bag3*^{fl/fl} mice brain slice culture by stimulating SCs with a train of 100-Hz stimuli (N=10-18). (B-E) Morris water maze test was performed. (B) Initial latency time to target was recorded during the 4-day training course. (C-E) In the probe trial test performed on Day 5, (C) initial latency to target; (D) number of target-crossing and (E) time spent in the target zone and other quadrants (NE, SE and SW) were recorded (N=13-18). The number of triplet alternation was recorded in both (F) T-maze and (G) Y-maze paradigms (N=13-18). (H) Elevated-plus maze test which assesses anxiety-like behavior was performed. Quantification of time spent in the open arm is shown (N=13-18). (I) Forced-swimming test which accesses depressive behavior was performed. Quantification of immobility time is shown (N=13-18). (J) Rotarod test which accesses

locomotor capabilities was performed. Quantification of latency time to fall is shown (N=13-18). (K) Open-field test which also accesses anxiety-like behavior and motor function was performed. Quantification of time spent in the field center is shown (N=13-18). Unless otherwise specified, all experiments were performed with at least 3 biological repeats; each individual assay was performed three times at least. * $P < 0.05$, ** $P < 0.01$, *** $P < 0.001$, ns=non-significant. Data represent the mean \pm SEM.

Journal Pre-proof



Supplementary Figure S6. BAG3 ectopic re-expression in AD-mouse rescued synaptic protein abundance. (A) Representative immunohistochemistry images showing changes in BAG3 signals in the hippocampal CA1 region of 5XFAD mice as compared to littermate controls (N=6). (B) Representative blots showing changes in levels of BAG3, HSP70 and selected synaptic proteins and their interactions in hippocampal samples harvested from 5XFAD mice stereotaxically injected AAV carrying expression vector of BAG3 or empty vector control. Quantification of relative band intensities is shown in (D) (N=6). Unless otherwise specified, all experiments were performed with at least 3 biological repeats; each individual assay was performed three times at least. *P<0.05, **P<0.01, ***P<0.001, ns=non-significant. Data represent the mean \pm SEM.



Supplementary Figure S7. Schematic diagram illustrating how CDK5 regulates BAG3 stability and hence the abundance of synaptic proteins. (A) Under normal circumstances, dynamic activation of CDK5 by p35 phosphorylates and promotes the degradation of BAG3. Reduced level of BAG3— a co-chaperone of HSP70—alleviates its inhibitory effect against HSP70-mediated degradation synaptic proteins, in particular, those take part in glutamatergic neurotransmission. It is therefore the extent and duration CDK5 activation corresponds to intracellular stimuli thus act as a master regulator synaptic abundance and function, hence strength of neurotransmission and fidelity of cognitive and memory functions. (B) In neuropathological conditions such as AD, A β triggers robust calpain-mediated cleavage of p35 to p25. P25 is more stable than p35 therefore this persistently activates CDK5. CDK5, under these scenarios, chronically phosphorylates and promotes BAG3 degradation. Sustained

reduction of BAG3, in contrast to its dynamic fluctuation under normal conditions, aberrantly unleashes HSP70 and favors its role in facilitating protein degradation. As HSP70 selectively targets glutamatergic synaptic components in neurons, loss of these proteins thus impairs glutamatergic firing which is crucial for facilitating memory formation and cognitive function.

Supplementary Table S1. List of phospho-peptides identified from SILAC (CDK5-P35 screen).

Supplementary Table S2. List of phospho-peptides identified from SILAC (P35 screen).

Supplementary Table S3. Lists of unique BAG3-interacting candidates identified from mass spectrometry and the corresponding list of enriched functions indicated by Gene Ontology and KEGG analyses.

Supplementary Table S4. Lists of unique HSP70-interacting candidates identified from mass spectrometry and the corresponding list of enriched functions indicated by Gene Ontology and KEGG analyses.

Supplementary Table S5. Lists of common BAG3 and HSP70 interacting candidates identified from mass spectrometry and the corresponding list of enriched functions indicated by Gene Ontology and KEGG analyses.

See Supplement 2 (Excel files) for all supplemental tables

Supplemental References

1. Chow HM, Guo D, Zhou JC, Zhang GY, Li HF, Herrup K, et al. (2014): CDK5 activator protein p25 preferentially binds and activates GSK3beta. *Proc Natl Acad Sci U S A.* 111:E4887-4895.
2. Johnson D, Boyes B, Fields T, Kopkin R, Orlando R (2013): Optimization of data-dependent acquisition parameters for coupling high-speed separations with LC-MS/MS for protein identifications. *J Biomol Tech.* 24:62-72.
3. Johnson D, Boyes B, Orlando R (2013): The use of ammonium formate as a mobile-phase modifier for LC-MS/MS analysis of tryptic digests. *J Biomol Tech.* 24:187-197.
4. Pimienta G, Chaerkady R, Pandey A (2009): SILAC for global phosphoproteomic analysis. *Methods Mol Biol.* 527:107-116, x.
5. Francavilla C, Hekmat O, Blagoev B, Olsen JV (2014): SILAC-based temporal phosphoproteomics. *Methods Mol Biol.* 1188:125-148.
6. Kim JY, Grunke SD, Levites Y, Golde TE, Jankowsky JL (2014): Intracerebroventricular viral injection of the neonatal mouse brain for persistent and widespread neuronal transduction. *J Vis Exp.* 51863.
7. Chow HM, Cheng A, Song X, Swerdel MR, Hart RP, Herrup K (2019): ATM is activated by ATP depletion and modulates mitochondrial function through NRF1. *J Cell Biol.*
8. Bankston AN, Ku L, Feng Y (2017): Active Cdk5 Immunoprecipitation and Kinase Assay. *Bio Protoc.* 7.
9. Bermejo MK, Milenkovic M, Salahpour A, Ramsey AJ (2014): Preparation of synaptic plasma membrane and postsynaptic density proteins using a discontinuous sucrose gradient. *J Vis Exp.* e51896.
10. Zhang J, Li H, Yabut O, Fitzpatrick H, D'Arcangelo G, Herrup K (2010): Cdk5 suppresses the neuronal cell cycle by disrupting the E2F1-DP1 complex. *J Neurosci.* 30:5219-5228.
11. Zhang J, Li H, Zhou T, Zhou J, Herrup K (2012): Cdk5 levels oscillate during the neuronal cell cycle: Cdh1 ubiquitination triggers proteasome-dependent degradation during S-phase. *J Biol Chem.* 287:25985-25994.
12. Zeng XC, Bhasin S, Wu X, Lee JG, Maffi S, Nichols CJ, et al. (2004): Hsp70 dynamics in vivo: effect of heat shock and protein aggregation. *J Cell Sci.* 117:4991-5000.
13. Shin JH, Yue Y, Duan D (2012): Recombinant adeno-associated viral vector production and purification. *Methods Mol Biol.* 798:267-284.
14. Cribbs AP, Kennedy A, Gregory B, Brennan FM (2013): Simplified production and concentration of lentiviral vectors to achieve high transduction in primary human T cells. *BMC Biotechnol.* 13:98.
15. Sievers F, Wilm A, Dineen D, Gibson TJ, Karplus K, Li W, et al. (2011): Fast, scalable generation of high-quality protein multiple sequence alignments using Clustal Omega. *Mol Syst Biol.* 7:539.

16. Leng L, Zhuang K, Liu Z, Huang C, Gao Y, Chen G, et al. (2018): Menin Deficiency Leads to Depressive-like Behaviors in Mice by Modulating Astrocyte-Mediated Neuroinflammation. *Neuron*. 100:551-563 e557.
17. Nunez J (2008): Morris Water Maze Experiment. *J Vis Exp*.
18. Ennaceur A, Delacour J (1988): A new one-trial test for neurobiological studies of memory in rats. 1: Behavioral data. *Behavioural brain research*. 31:47-59.
19. Powell CM, Schoch S, Monteggia L, Barrot M, Matos MF, Feldmann N, et al. (2004): The presynaptic active zone protein RIM1alpha is critical for normal learning and memory. *Neuron*. 42:143-153.

Journal Pre-proof